Olisthodiscus represents a new class of Ochrophyta

Dovilė Barcytė[1]

Department of Biology and Ecology, Faculty of Science, University of Ostrava, 710 00 Ostrava, Czech Republic

Wenche Eikrem[1,2]

Norwegian Institute for Water Research, Gaustadallèen 21, 0349 Oslo, Norway

University of Oslo, Department of Biosciences, P.O.box 1066 Blindern, 0316 Oslo, Norway

Anette Engesmo

Norwegian Institute for Water Research, Gaustadallèen 21, 0349 Oslo, Norway

University of Oslo, Department of Biosciences, P.O.box 1066 Blindern, 0316 Oslo, Norway

Sergio Seoane

University of the Basque Country (UPV/EHU), Department of Plant Biology and Ecology, 48940 Leioa, Spain

Jens Wohlmann

University of Oslo, Department of Biosciences, P.O.box 1066 Blindern, 0316 Oslo, Norway

Aleš Horák

Biology Centre, Czech Academy of Sciences, Institute of Parasitology, Branišovská 31, 37005, České Budějovice, Czech Republic.

Department of Molecular Biology, Faculty of Science, University of South Bohemia, Branišovská 31, 37005, České Budějovice, Czech Republic.

Tatiana Yurchenko

Department of Biology and Ecology, Faculty of Science, University of Ostrava, 710 00 Ostrava, Czech Republic

and Marek Eliáš[2]

Department of Biology and Ecology, Faculty of Science, University of Ostrava, 710 00 Ostrava, Czech Republic

[1]Co-first authors of the paper

[2]Authors for correspondence: Wenche Eikrem – wenche.eikrem@niva.no, Tel.: +47 98227737; Marek Eliáš – marek.elias@osu.cz, Tel.: +420 597 092 329

This article has been accepted for publication and undergone full peer review but has not been through the copyediting, typesetting, pagination and proofreading process, which may lead to differences between this version and the Version of Record. Please cite this article as doi: 10.1111/jpy.13155

Running title: *Olisthodiscus luteus* revisited

Editorial Responsibility: O. De Clerck (Associate Editor)

ABSTRACT

The phylogenetic diversity of Ochrophyta, a diverse and ecologically important radiation of algae, is still incompletely understood even at the level of the principal lineages. One taxon that has eluded simple classification is the marine flagellate genus *Olisthodiscus*. We investigated *O. luteus* K-0444, and documented its morphological and genetic differences from the NIES-15 strain, which we described as *O. tomasii* sp. nov. Phylogenetic analyses of combined 18S and 28S rRNA sequences confirmed that *Olisthodiscus* constitutes a separate, deep, ochrophyte lineage, but its position could not be resolved. To overcome this problem, we sequenced the plastid genome of *O. luteus* K-0444 and used the new data in multigene phylogenetic analyses, which suggested that *Olisthodiscus* is a sister lineage of the class Pinguiophyceae within a broader clade additionally including Chrysophyceae, Synchromophyceae, and Eustigmatophyceae. Surprisingly, the *Olisthodiscus* plastid genome contained three genes, *ycf80*, *cysT*, and *cysW*, inherited from the rhodophyte ancestor of the ochrophyte plastid yet lost from all other ochrophyte groups studied so far. Combined with nuclear genes for CysA and Sbp proteins, *Olisthodiscus* is the only known ochrophyte possessing a plastidial sulfate transporter SulT. In addition, the finding of a *cemA* gene in the *Olisthodiscus* plastid genome and an updated phylogenetic analysis ruled out the previously proposed hypothesis invoking horizontal *cemA* transfer from a green algal plastid into Synurales. Altogether, *Olisthodiscus* clearly represents a novel phylogenetically distinct ochrophyte lineage, which we have proposed as a new class, Olisthodiscophyceae.

Key index words: morphology; phylogeny; plastid genome; pigments; Ochrophyta; *Olisthodiscus*; Raphidophyceae; SulT; rDNA; taxonomy

Abbreviations: ER, endoplasmic reticulum; GDV, Golgi-derived vesicle;

INTRODUCTION

Ochrophyta, or the plastid-bearing stramenopiles, are one of the largest radiations of algae (Andersen 2004, Brown and Sorhannus 2010, Yang et al. 2012). They most likely emerged by a higher-order (secondary or tertiary) endosymbiotic event featuring a heterotrophic stramenopile host and an endosymbiont that was a red alga or an organism with a rhodophyte-derived secondary plastid (Dorrell et al. 2017, Sibbald and Archibald 2020). The descendants of the ochrophyte

ancestor have diversified into a broad spectrum of morphological and physiological forms, from unicellular to complex multicellular types. Classifying this extreme diversity has proved to be a real challenge, but the advent of new approaches, historically including transmission electron microscopy (with investigations of the flagellar apparatus considered particularly informative about the phylogenetic relationships), pigment analyses, molecular phylogenetics, and most recently phylogenomics, has enabled the drawing of a progressively refined picture of the ochrophyte phylogeny at all levels, including that of the main clades and their relationships (Yang et al. 2012, Derelle et al. 2016). However, numerous historically described photosynthetic stramenopiles have not yet been studied using the aforementioned modern taxonomic methods, and the cataloguing of ochrophyte diversity is far from finished as novel lineages are still being discovered, even such that become classified as new classes (Horn et al. 2007, Kai et al. 2008, Wetherbee et al. 2019). Furthermore, the branching order of the main ochrophyte lineages is not yet robustly defined, as is obvious from discrepancies between results obtained by different types of data analysed, such as plastid versus nuclear genes (Derelle et al. 2016, Noguchi et al. 2016, Han et al. 2019, Ševčíková et al. 2019).

An interesting candidate for a phylogenetically novel ochrophyte is *Olisthodiscus luteus*, the type species of the genus *Olisthodiscus* originally described from a brackish pool on the Isle of Wight, the United Kingdom, and presented with a detailed description and colored line drawings (Carter 1937). Two additional *Olisthodiscus* species were described from shallow waters on the East Coast of North America: *O. magnus* and *O. carterae* (Hulburt 1965). However, *O. carterae* was later recognized as conspecific with *Heterosigma akashiwo,* and the name regarded invalid, while *O. magnus* was considered probably conspecific with *Chattonella marina* (Hallegraeff and Hara 2003), rendering *Olisthodiscus* presently monospecific. On a number of occasions, *O. luteus* has been confused with *H. akashiwo* (e.g., in Leadbeater 1969 and Gibbs et al. 1980). In contrast to the pelagic *Heterosigma, Olisthodiscus* is usually associated with shallow waters and sandy shores, and has been reported from salt marshes and beaches in Europe, South Africa, North America and Japan (Fukuyo et al. 1990, Hallegraeff and Hara 2003). It has been observed as far north as in the sandy shores of Magdalenefjorden, Spitzbergen (W. Eikrem, unpub. data). Its benthic preferences are reflected in its dorso-ventrally flattened cells and mode of swimming; it glides flat on the substrate, as opposed to the pelagic *Heterosigma* that has very little dorso-ventral compression and rotates while swimming.

The taxonomic affiliation of *Olisthodiscus* has been a matter of controversy, and following careful consideration it was assigned to the Xanthophyceae by Carter (1937). After studying the ultrastructure of the strain NIES-15 isolated from the Seto Inland Sea, Japan, and identified as *O. luteus*, Hara et al. (1985) concluded that it was most appropriate to confine *Olisthodiscus* to the Raphidophyceae. However, Christensen (1980, 1994) ascribed great importance to pigments and placed *Olisthodiscus* together with *Heterosigma* and *Chattonella* in the Chrysophyceae, noting that *Olisthodiscus* differs from *Heterosigma* and *Chattonella* in lacking ejectile organelles and having a yellowish color. Indeed, the flagellar root system of *Olisthodiscus* (NIES-15) has more features in common with chrysophytes and brown algae than raphidophytes (Vesk and Moestrup 1987, Inouye et al. 1992). However, Inouye et al. (1992) did not accept the arguments for classifying *Olisthodiscus* in Chrysophyceae and preferred a view of Raphidophyceae as a group encompassing extremely diverse organisms in terms of flagellar apparatus organization, with *Olisthodiscus* occupying a discrete position within the class.

Oddly, the application of molecular phylogenetic approaches to resolving the phylogenetic position of *Olisthodiscus* has been somewhat inconsequential. The first DNA sequences published with the attribution to *O. luteus* (Boczar et al. 1989, Delaney and Cattolico 1989, 1991) in fact come from a misidentified *Heterosigma akashiwo* (Table 1). The very first DNA sequence genuinely derived from *Olisthodiscus*, a partial 28S rRNA gene sequence from the NIES-15 strain, was deposited to GenBank in 1998 by L. Connell (Table 1), but there is no publication associated to the record. The first molecular phylogenetic analysis including *Olisthodiscus* was probably reported in a Master's thesis by Tyrrell (1999). Strikingly, on the basis of sequencing the 18S rRNA gene he proposed that *O. luteus* be classified into a new class denoted "Olisthophyceae". However, these results and formal description of the class were not subsequently published in a peer-reviewed journal, and the sequence was not released to a database. Later, Tyrrell et al. (2001) and Bowers et al. (2006) reported partial 28S rRNA and 18S rRNA gene sequences, respectively, attributed to the *O. luteus* strain NIES-15 (Table 1), but they did not use them for phylogenetic analyses and the position of *O. luteus* was not discussed in the respective papers. A note then appeared in two papers by Yamaguchi et al. (2008, 2010) stating that, based on their unpublished analyses of 18S rRNA sequence data, *O. luteus* is not a raphidophyte. However, no publication that would provide further details on their findings has appeared since then.

When the first phylogenetic trees that included the available 18S rRNA gene sequence (AY788937.1) from *Olisthodiscus luteus* NIES-15 were finally published by others, this organism

appeared as an isolated branch outside Raphidophyceae or any other conventionally defined ochrophyte class (Přibyl et al. 2012, Cavalier-Smith and Scoble 2013). Based on this, Cavalier-Smith assigned *O. luteus* to a newly erected subclass Sulcophycidae, and placed it along with pelagophytes and dictyochophytes (treated together as the subclass Alophycidae) into his class Hypogyristea, despite the arguably insignificant bootstrap support for the monophyly of this class (Cavalier-Smith and Scoble 2013). According to the description, the subclass Sulcophycidae embraces naked cells with a groove running the length of the cell where the smooth flagellum is located, a flagellar transition zone with two rings below the dense plate, plastids with girdle lamellae, fucoxanthin, and protruding pyrenoids not traversed by thylakoids. The subclass includes the single order Olisthodiscales with a single family Olisthodiscaceae, but Cavalier-Smith and Scoble (2013) proposed that *Sulcochrysis biplastida* (described by Honda et al. 1995) possibly also belongs in the Sulcophycideae, although this could not be confirmed due to lack of DNA sequences from this organism.

In this paper we demonstrate a previously unknown genetic and morphological variation within *Olisthodiscus* and conclude that the previously investigated strain from Japan identified as *O. luteus* is in fact a separate species, which we here formally describe. We revisit the taxonomic placement of *Olisthodiscus* within Ochrophyta by employing additional molecular data, including a large dataset of plastid genes, which clearly show an isolated position of this genus consistent with it representing an ochrophyte class of its own. Furthermore, we report on the sequencing and detailed analysis of the plastid genome of *O. luteus* strain K-0444, which revealed several unexpected features and improved our understanding of the evolution of ochrophyte plastid genomes in general.

MATERIALS AND METHODS

Algal cultures, growth conditions, light microscopy.

The cultures used in this study, K-0444, isolated from the Nivå Bugt, The Sound, Denmark, and the already mentioned NIES-15, were obtained from the Scandinavian Culture Collection of Algae and Protozoa (SCCAP) and National Institute for Environmental Studies (NIES), respectively. They were grown in CCALA brackish water (https://ccala.butbn.cas.cz/en/brackish-water), placed in a cooling box (Helkama, Helsinki, Finland) at 16°C, under continuous light provided by a cool white OPPLE LED 28W tube (Eindhoven, Netherlands). The strains were subcultured once every two weeks. For the work done at the University of Oslo (SEM on both strains and TEM on K-

0444), the strains were cultivated under a 12:12 h light:dark cycle, and illumination of 100 µmol photons · m^{-2} · s^{-1}. The media used were IMR½ (salinity of 34) for K-0444 and ES (salinity of 20) for NIES-15; for media recipes, we refer to Andersen (2005). The cultures were examined using an Olympus (Tokyo, Japan) BX53 light microscope with differential interference contrast (DIC); microphotographs were captured with an Olympus DP73 camera and cells were measured using the Olympus cellSens Dimenion 1.6 software.

SEM.

Strains NIES-15 and K-0444 were prepared for SEM by transferring cells to fresh medium approximately one week before fixation, to ensure healthy and dense algal strains in an exponential growth phase. Osmium tetroxide, OsO_4, (Sigma-Aldrich, St. Louis, MO, USA) was diluted with sterile filtered seawater of the same salinity as the strains' growth media. Algal cells were added to OsO_4 to a final concentration of 1% and left in the tube to settle for one hour. Samples were mounted on glass cover slips covered in poly-L-lysin (Sigma-Aldrich, St. Louis, MO, USA) and left to settle for an additional hour. All samples were rinsed 5 times in seawater of corresponding salinity, followed by two rinses in distilled water. Dehydration was performed with 6 steps in an ethanol series ranging from 30-100%. All incubations lasted 20 min, followed by a 10 min intermediate incubation where new ethanol concentration was added to the old. The final step of 100% was repeated four times. Samples were critically point dried (CPD) using a Bal-Tec CPD 030 Critical Point Dryer (Los Angeles, USA), sputter coated in a Cressington 308UHR (Watford, England) with 4-9 nm of platinum, and examined in a S-4800 Hitachi Field Emission SEM (Tokyo, Japan).

TEM.

Live cultures of K-0444 were concentrated approximately tenfold by filtration through a 4 µm cellulose acetate filter on filter paper. The concentrated cultures were left at incubation conditions (ca. 15°C) for about 20 min to recover before fixation. They were then placed into cellulose capillaries (M. Wohlwend GmbH) according to Hohenberg et al. (1994) and cryofixed in a Leica HPM100 High Pressure Freezer. The substitution was done using a Bal-Tec FSU010 Freeze Substitution Unit, starting with incubation for 45 h at -90°C in 0.1% tannic acid (Malinckrodt Lot. 8835) in acetone and in 1% uranylacetate, 2% OsO_4 in acetone for the surface coat contrasting and the intracellular ultrastructure, respectively. This was followed by three washes each for 15 min

with acetone at -90°C, and a 9 h incubation with 1% uranylacetate, 2% OsO_4 in acetone at -50°C. 0.5% glutaraldehyde, along with 0.5% water were added to the substitution mix at -50°C, followed by an incubation for 3 h at -40°C, 8 h at -30°C and 3 h at -20°C. After washing three times for 15 min with acetone, 2% OsO_4 in acetone was added followed by a gradual increase to 0°C for increased Osmium contrasting (Wild et al. 2001) as follows: 3 h at -10°C, 3 h at -5°C, 1h at 0°C. After three washes each for 15 min with acetone, the samples were cooled to -20°C, and after removal of the last washing step, ca. 25°C warm 25% EPON (Sigma) in acetone was added for 15 h infiltration on a rotating wheel in open vials followed by a 24 h incubation with pure EPON (3[DDSA]:7[NMA], 1% DMP-30). Polymerization in flat embedding moulds containing fresh EPON was at 60°C for 48 h, sectioning was done at 55 nm thickness using a Leica UCS microtome. The sections were stained with 4% uranylacetate in water for 20 min, and lead citrate (Reynolds 1963) for 90 sec. Imaging was done on a Jeol JEM-1400 at 120 kV using a Tvips 216 camera.

Live cells of NIES-15 were gently centrifuged and immersed in a cryoprotectant (20% BSA in cell medium) and immediately frozen with a Leica HPM100 high-pressure freezer (Leica Microsystems, Vienna, Austria). The cells were freeze substituted in 2% OsO_4 and 100% acetone using an automatic freeze substitution system Leica EM AFS2. The sample was then washed three times in 100% acetone followed by a gradual embedding in EMbed-812 resin at room temperature (resin:acetone – 1:2, 1:1, and 2:1 for one hour per each) with a final overnight embedding in 100% resin. The sample was then embedded into a fresh degassed resin and polymerized at 60°C for 48 h. Thin sections were cut on a Reichert-Jung Ultracut E ultramicrotome and stained using uranyl acetate and lead citrate. Sections were examined and photographed using a JEOL JEM-1011 (Tokyo, Japan) electron microscope, equipped with a Veleta camera and the iTEM 5.1 software (Olympus Soft Imaging Solution GmbH).

DNA sequencing and assembly.

To obtain rDNA sequences from the NIES-15 strain, the culture was harvested in the exponential growth phase and DNA was isolated using a NucleoSpin® Plant II Mini Kit (Macherey-Nagel, Germany), following the manufacturer's instructions. PCR reaction volumes were 25 µL; 12.5 µL GoTaq mastermix (Promega, Madison, WI, USA), 5 µM primers, 9 µL dH_2O and 0.5 µL DNA template. The PCR was run in a Thermo Mastercycler (Eppendorf, Hamburg, Germany) with the following conditions: 3 min initial denaturation at 94˚C followed by 35 cycles of 45 s at 94˚C, 45 s

at 55˚C and 1 min at 73˚C with a concluding elongation step for 5 min at 73˚C. The resulting PCR-products were tested on a 2% agarose gel with GelRed (Biotium, Hayward, CA, USA). All PCR and sequencing primers are listed in Table S1 in the Supporting Information. PCR products were cleaned using ExoSAP-IT (Affymetrix, Santa Clara, CA, USA) and diluted 1:10 with PCR grade water (Promega). Sanger sequencing was performed by GATC (Konstanz, Germany). A continuous sequence comprising the 18S rRNA gene, the ITS regions (including the 5.8S rRNA gene), and a part of the 28S rRNA gene was assembled and edited in Geneious v.7.1.1 (Biomatters). The sequence was deposited as GenBank accession number KP780272.1.

Genomic DNA of *Olisthodiscus luteus* K-0444 was isolated using an Invisorb® Spin Plant Mini Kit (STRATEC Molecular GmbH, Berlin, Germany), following the manufacturer's instructions. The isolated DNA was sequenced using the NovaSeq 6000 technology by Macrogen Inc. (Seoul, South Korea), yielding 51,134,674 reads. These were trimmed by Trimmomatic v.0.36 (Bolger et al. 2014), leaving 49,966,152 high-quality reads for the genome sequence assembly achieved by using SPAdes v.3.5.0 (Bankevich et al. 2012). Four scaffolds were identified by blast searches (Altschul et al. 1997) with common plastid proteins as presumably corresponding to the plastid genome, with two having the read coverage roughly twice as high (965× and 895×) as the other two (453× and 533×). This suggested a conventional plastid genome architecture with two copies of the inverted repeat separated by single-copy regions. Scaffolds were joined manually with the recruitment of additional reads to obtain a complete circular-mapping sequence. The resulting assembly was validated by mapping reads with Bowtie2 v.2.3.4.1 (Langmead and Salzberg 2012), with the mapping inspected in Tablet v.1.14.04.10 (Milne et al. 2013). The *O. luteus* K-0444 plastid genome sequence was deposited as GenBank accession number MT859097.1. In addition, the region representing the full rDNA operon was identified in one of the scaffolds, extracted, and deposited as GenBank accession number MW045617.1.

Annotation of the plastid genome and comparative analyses.

The complete *Olisthodiscus luteus* plastid genome sequence was initially annotated by using MFannot (http://megasun.bch.umontreal.ca/cgi-bin/dev_mfa/mfannotInterface.pl). The proposed gene modes and their identities were carefully checked manually and adjusted on the basis of multiple sequence alignments with homologs from other taxa and database searches with blast, HHpred (Zimmermann et al. 2018) and Phyre2 (Kelley et al. 2015). A few short or poorly

conserved genes completely missed by MFannot (*secG*, *rrn5*, *ssrA*, and the intron-containing gene *trnL(UAA)*) were identified manually (in case of the non-coding RNA-specifying genes with the aid of RFAM search; Kalvari et al. 2018) and integrated into the genome annotation. A graphical map of the plastid was prepared using OGDRAW v.1.3.1 (https://chlorobox.mpimp-golm.mpg.de/OGDraw.html; Greiner et al. 2019). For comparison of the plastid gene complement of *O. luteus* with those of other ochrophytes (Table S2 in the Supporting Information), we expanded the data presented in Ševčíková et al. (2019) by integrating occurrences of genes in the newly sequenced plastid genomes of three selected members of Synurales (Kim et al. 2019) and four dictyochophytes (Han et al. 2019). We updated the existing genome annotations for some of the taxa, since we noticed some genes were missed by the respective authors. In a few cases we even detected apparent sequencing or assembly issues behind the missing annotations, specifically single-nucleotide indels introducing frame-shifts in the respective coding sequences. Homologs of genes of interest presumably encoded by the nuclear genomes of the taxa concerned were searched by tblastn against the respective transcriptome assemblies, including the ones publicly available (those in the TSA division of the GenBank database and those generated by the MMETP project; Keeling et al. 2014) as well as our unpublished transcriptome assembly from *O. luteus* K-0444. Relevant sequences (transcripts encoding GapC1, GapC2, CysA, and Sbp proteins) were extracted from the *O. luteus* assembly and deposited as GenBank accession numbers MW052523.1, MW052524.1, MT497912.1 and MT497913.1, respectively.

Phylogenetic analyses of rRNA sequences.

18S and 28S rDNA (rRNA) sequences were compiled from public sources (in some cases including genome or transcriptome assemblies) for representatives of all major ochrophyte classes (Table S3 in the Supporting Information). To maximize taxonomic sampling, we included 28S rRNA/rDNA sequences extracted from our unpublished genome assembly of the eustigmatophyte *Trachydiscus minutus* and the transcriptome assembly for the non-photosynthetic ochrophyte *Picophagus flagellatus* (separate class Picophagea); these sequences were deposited as GenBank accession numbers MW045558.1 and MW045538.1, respectively. No 28S rRNA sequence data was available for a few minor classes (Chrysomerophyceae, Aurearenophyceae) that are certainly not directly related to *Olisthodiscus*, so these were ignored in the analysis. However, we included two environmental 18S rDNA clones with close affinities to *Olisthodiscus*, treating the corresponding unavailable 28S rDNA sequences as missing data. Sequences were aligned using

MAFFT v.7.450 (Katoh and Standley 2013) with the E-INS-i option, the alignments were trimmed with trimAl v.1.2 using the *–gappyout* option (Capella-Gutierrez et al. 2009), and concatenated with FASTconCAT-G v.1.04 (Kück and Longo 2014), yielding a final two-gene alignment encompassing 4,802 aligned positions. The maximum likelihood (ML) tree was inferred using IQ-TREE v.1.5.3. (Nguyen et al. 2015) with a partitioned dataset, applying the TN+F+I+G4 model for the 18S data and TIM2+F+I+G4 for the 28S data as suggested by ModelFinder using the BIC criterion (Kalyaanamoorthy et al. 2017) implemented in IQ-TREE. A Bayesian estimation of the phylogeny was performed with MrBayes v.3.2.7a (Ronquist and Huelsenbeck 2003) with partitioned data and GTR+G+I model applied for both partitions. MCMC analysis was performed with two runs of eight chains for 1,000,000 generations. For the analysis, 2,500 samples were discarded as burnin. A supplementary phylogenetic tree of 18S rDNA sequences encompassing all so far sequenced Raphidophyceae and Pinguiophyceae species was also computed as described above.

Screening of metabarcoding and metagenomic data.

The global distribution of *Olisthodiscus* was screened in BioMarKs (European coastal waters; Logares et al. 2014) and the Tara Oceans (mostly tropic to temperate oceans; de Vargas et al. 2015) V9 metabarcoding datasets. To account for possible PCR biases, we also used metagenomic Malaspina miTag datased (Obiol et al. 2020). All these databases were screened using blast with *Olisthodiscus* 18S rRNA as a search query. Sequences of the top blast hits were then evaluated by comparing them with blastn against the NCBI non-redundant nucleotide sequence database to exclude those that match organisms unrelated to *Olisthodiscus*. Three candidates that passed this filter were aligned to a reference alignment of ochrophyte 18S rRNA sequences (the one used in the analyses described in the previous section) using the PaPaRa (https://cme.h-its.org/exelixis/web/software/papara/index.html), and their most likely position in ochrophyte phylogeny was assessed using the EPA algorithm as implemented in RAxML (Berger et al. 2011).

ITS2 rDNA secondary structure analysis.

ITS2 secondary structures of the two *Olisthodiscus* strains NIES-15 and K-0444 were computed using RNAstructure web server (Bellaousov et al. 2013) employing the PARTS algorithm v.6.0.1 predicting the common secondary structure, including base pair probabilities, for two unaligned sequences (Harmanci et al. 2008). The predicted secondary structures were inspected and

manually modified using 4SALE v.1.7 (Seibel et al. 2008). The same software was applied to build the sequence-structure alignment and search for compensatory base changes (CBCs).

Phylogenetic analyses of plastid genes.

A matrix of 69 conserved plastid-genome encoded proteins was built by updating alignments used previously by Ševčíková et al. (2019). For the new analysis, the ClpC protein was removed (because of its complicated history of splitting in some ochrophytes) and replaced by two different proteins, RbcL and CbbX (all genes used in this analysis are highlighted in Table S2). Homologs were identified by the gene name in respective genome annotations or by blast. Since there is no plastid genome sequence available for a representative of Synchromophyceae, we exploited the transcriptome assembly generated for *Synchroma pusillum* strain CCMP3072 by the MMETSP project. Transcripts putatively derived from the plastid genome were identified by tblastn searches and are listed in Table S4 in the Supporting Information (their assignment to the plastid rather than nuclear genome was frequently supported by the fact that they were polycistronic, with coding sequences of multiple typical plastid genes). We similarly tried to obtain plastid genome-derived sequences from the existing transcriptome assemblies from the pinguiophytes *Pinguiococcus pyrenoidosus* CCMP2078 and *Phaeomonas parva* CCMP2877, but they proved to include very few candidates. Multiple alignments were created separately for each conserved protein and carefully inspected to ensure that orthologous sequences were included for all species. Final alignments were created by using MAFFT employing the E-INS-i strategy and processed as described above for the rDNA sequence alignments, yielding a supermatrix of 17,531 aligned amino acid positions. The ML tree was inferred from the supermatrix by using IQ-TREE, the PMSF approximation (Wang et al. 2018) with the LG+C60+F+G mixture model, and 100 non-parametric bootstraps. The Bayesian phylogenetic reconstruction was carried out for the same supermatrix using PhyloBayes MPI v.1.8 (Lartillot et al. 2013) and the substitution model CAT-GTR. Two independent Markov Chain Monte Carlo (MCMC) chains were run with 13,818 and 13,795 iterations, respectively. Convergence was assessed using the *bpcomp* (subsampling every 10th iteration) and *tracecomp* tools implemented in PhyloBayes, with 2,000 samples discarded as burnin in each analysis.

A dataset based on a smaller number of plastid genes, yet including some critical taxa missing in the 69-protein supermatrix, was built by combining amino acid sequences of five plastid genome-encoded proteins (*Rbc*L, *Psa*A, *Psb*A, *Psb*C, *Cbb*X) with nucleotide sequences of

plastid 16S and 23S rRNA genes. Where a species had no complete published plastid genomes, we used individual gene sequences available in GenBank (mostly from Yang et al. (2012)) or sequences extracted from available transcriptome assemblies (Table S4). Sequence alignments were built and processed as described above to create a supermatrix consisting of 6,536 aligned positions including both nucleotides (4,211 positions) and amino acids (2,325 positions). The ML tree was inferred using IQ-TREE applying the GTR+F+R5 model for nucleotide sequences and the LG+R5 model for amino acids as suggested by the programme. Support values were inferred using non-parametric 100 bootstrap replications.

Phylogenetic analyses of individual proteins of special interest (CemA, CysT, CysW, CysA, and Spb) were carried out with generally same strategy as aforementioned multigene analyses. Homologs were identified with blastp and selected to provide a representative sampling of the respective families. Alignments were built using MAFFT, trimmed manually or using trimAl to remove poorly conserved regions, and subjected to tree inference with IQ-TREE with the best-fitting model selected by the programme (the models are specified in legends to the respective figures).

All resulting trees were visualized with FigTree v.1.4.2 (Rambaut 2009) and further edited with Inkscape v.0.91. All alignments used in this study are available upon request from the corresponding author ME.

Pigment analysis.

10 mL of exponentially growing culture of strains K-0444 and NIES-15 was vacuum filtered onto 47 mm Whatman GF/F glass fibre filters and kept frozen at -20°C until used. Frozen filters were extracted under low light in 3 mL 90% acetone, grounding with a glass stick. The resulting slurry was removed with a syringe filter (0.2 μm pore size) and the filtrate obtained was analyzed by HPLC based on the method described by Zapata et al. (2000), following the steps explained in Seoane et al. (2009).

RESULTS

Morphology and ultrastructure.

The two studied *Olisthodiscus* strains, K-0444 and NIES-15, had a similar gross morphology (Fig. 1). Cells were round, broadly ellipsoidal or ovate, prominently flattened, dorsally convex and ventrally concave. The algae possessed two unequal flagella, emerging sub-anteriorly or nearly

centrally from a ventral funnel-shaped depression (Fig. 1, B and E). The longer anteriorly directed flagellum lashed rapidly and pulled the cell forward while the shorter posterior flagellum trailed behind. The cells did not rotate while swimming but glided with the ventral side directed upwards while in motion. Both strains had multiple plastids, ranging typically from five to twelve, and varying in size. They were arranged peripherally, and pyrenoids were sometimes visible as well (Fig. 1, B and M). A prominent nucleus with a discernible nucleolus was situated in the cell centre or anterior (Fig. 1, A–C, F and O). One to two conspicuous orange or red extraplastidial globules were also present in both strains (Fig. 1, A, C, M, O and U). Occasionally, the globule appeared colourless. Sometimes the cells lost their definite form and became sluggish. Formation of a "pseudopodium" containing a plastid was also observed (Fig. 1I). Particularly older cultures contained cells with shrunken plastids (Fig. 1J). Internal vesicles arranged in a honeycomb pattern were also commonly encountered (Fig. 1, K and R–T). Often the cells were covered by two forms of colourless appendages: crenate or terminally beaded thread-like (Fig. 1, D, P and S–U).

Asexual reproduction by longitudinal fission, including nucleus and flagella duplication was observed (Fig. 1, G and Q). The subsequent separation of two daughter cells was also conspicuous (Fig. 1, H and R). In addition, biflagellate cells resembling zoospores and containing one or two plastids were also detected (Fig. 1, V and W). They were formed in an enlarged vegetative cell divided by prominent septa (Fig. 1L). Cell lysis occurred by rupture of one cell end and release of the cytoplasmic contents, leaving plastid rings as debris (Fig. 1X). The vegetative cell size of both strains was similar, K-0444 having cells 7–15 µm long and 5–10 µm wide (n=85), and NIES-15 possessing cells 9–16 µm in length and 5–10 µm in width (n=80). Old globular cells reached up to 25 µm in diameter it both strains.

Despite being generally alike, K-0444 and NIES-15 showed slight morphological differences. For example, cells of NIES-15 were more laterally compressed, giving them an acute ellipsoidal form and making them slightly longer (Fig. 1N). Secondly, the extraplastidial globule was extremely big (up to 3.5 µm in diameter) and had a red colour in the cells of NIES-15, while in K-0444 it was smaller (usually 1.5 µm, only occasionally up to 3 µm in diameter) and typically orange.

Investigation of both strains in SEM (Fig. 2) showed that the anterior flagellum had hairs and the posterior flagellum was smooth (Fig. 2, A, B and E). In K-0444, a swelling located at the base of the longer tinsel flagellum was also observed (Fig. 2D). Both flagella emerged from a shallow depression on the ventral side (Fig. 2, A, D and F). In both strains the cell surface was covered by

small scales, fibrils, and bead-like protrusions (Fig. 2, C and E–G). Moreover, some of the latter structures also had stalks.

Examination of K-0444 using TEM (Fig. 3) revealed a number of ultrastructural similarities to NIES-15 previously investigated in detail by Hara et al. (1985) and Inouye et al. (1992). The plasmalemma of K-0444, like that of the NIES-15 strain, was covered in scales (Fig. 3, A–C). They were typically arranged in a single layer and interconnected by fibres (Fig. 3A). Scales were composed of seven or eight irregular pentagonal plates stacked in a rod-like structure (Fig. 3, D and E). The pentagonal plates were about 50 nm in diameter and the length of the stack reached up to 150 nm. Scales were produced by the Golgi apparatus and delivered by Golgi-derived vesicles (GDVs) to the cell's surface (Fig. 3F). Numerous peripheral vesicles were sandwiched between the plasmalemma and plastids, often filled with electron-dense granules, and interconnected by bridges (Fig. 3, A and B). The stalked protrusions found on the surface also contained granular material. Microtubules, were arranged in a single row and underlaid the peripheral vesicles on both lateral sides (Fig. 3A). At each side of the basal bodies, membranous structures were found (Fig. 3, A and C). The anterior flagellum bore mastigonemes and scales (Fig. 3, G and H). Mastigonemes associated with the endoplasmic reticulum (ER) were also observed in the cytoplasm (Fig. 3C).

Our additional examination of NIES-15 (Fig. 4) confirmed the similarity of the fine structural features of the two strains (Fig. 4, A–C). Nevertheless, we also observed features not noticed in K-0444 or not reported in previous investigations of the NIES-15 strain. Notably, cells, particularly zoospores, can be covered by several layers of scales (Fig. 4D), and the scales were typically composed of five or six pentagonal plates (Fig. 4, E and G). Moreover, some of the scale stacks were attached to each other and formed double scales (Fig. 4H). Some cells contained internal vesicles filled with an amorphous material (Fig. 4F). Membranous structures from which the peripheral vesicles putatively arose were also conspicuous (Fig. 4G).

Genetic diversity of isolates.

All *Olisthodiscus* DNA sequences currently available in GenBank were compared to the sequences generated for this study (Table 1), clearly revealing two genotypes of *Olisthodiscus*. Strikingly, it turned out that the two sequences previously deposited to GenBank by Bowers et al. (2006) as 18S rRNA and the ITS1-5.8S rRNA-ITS2 region from the NIES-15 strain (accession numbers AY788937.1 and DQ065612.1, respectively) are in fact of the K-0444 genotype,

suggesting a problem with the cultures used. The 18S rRNA genes of the two genotypes differed by eight substitutions and two one-nucleotide indels, whereas the region of the 28S rRNA gene available for comparison (635 aligned positions) was more variable and exhibited 50 substitutions and five one-nucleotide indels. Sequences of the ITS2 region are even more differentiated between the strains K-0444 and NIES-15, exhibiting only 76.18% identity. Predicted ITS2 rRNA secondary structures of the two genotypes (Fig. S1 in the Supporting Information) showed the common ITS2 motifs encountered among eukaryotes (i.e., four helices with the third being the longest and the most variable one, and helix II containing the 'U-U' mismatch; Schultz et al. 2005). On the contrary, helix III was branched as previously also found in other ochrophyte algae (e.g., eustigmatophytes; Kryvenda et al. 2018). Differences in the ITS2 sequences of the two *Olisthodiscus* strains mapped onto the predicted secondary structure of the NIES-15 ITS2 region uncovered four CBCs (Fig. S1). A single CBC was found in helix II (i.e., an 'A-U' pairing in NIES-15 exchanged for 'U-G' in K-0444 close to the terminal loop). Simultaneously, helix III contained three CBCs, i.e., pairings 'U-A', 'A-U' and 'G-U' in NIES-15 exchanged, respectively, for 'C-G', 'G-C', and 'U-A' in K-0444 (Fig. S1). Comparison of a previously reported partial *rbcL* gene sequence from the NIES-15 strain (Iida et al. 2007) with the *rbc*L sequence obtained by us as part of the full plastid genome of the strain K-0444 revealed 57 substitutions in the region compared (1,375 bp; i.e., only 95.9% identity). Most of the substitutions are at synonymous positions, but some do cause changes in the encoded amino acid, translating into 11 differences in the amino acid sequences (out of 457 compared). We also compared the two partial sequences of the nuclear GapC1 and GapC2 genes previously reported from the NIES-15 strain (Takishita et al. 2009) with the corresponding orthologs extracted from our unpublished transcriptome assembly for the strain K-0444. The respective coding sequences differed by 96 mismatches (out of 898 positions; 89% identity) in the case of GapC1 and by 163 mismatches (out of 913; 82% identity) in the case of GapC2.

Occurrence of Olisthodiscus *assessed by an analysis of environmental DNA surveys.*

The existence and distribution of *Olisthodiscus*-related organisms were evaluated by investigating data from three large environmental DNA surveys of marine habitats. The Tara Oceans V9 metabarcoding dataset is the most comprehensive metabarcoding collection of planktonic communities and targets mostly open tropics to temperate oceans (de Vargas et al. 2015). In contrast, the BioMarKs project focuses on the European coastal shelf waters while using the same

V9 marker (Logares et al. 2014). These datasets are based on high-throughput amplicon sequencing. To reduce the possibility of PCR bias, which would under- or over-represent the *Olisthodiscus* counts, we also screened the metagenomic Malaspina expedition miTags (Obiol et al. 2020). No barcodes identical or closely similar to *Olisthodiscus* 18S rRNA sequence were retrieved from any of the aforementioned datasets, suggesting that this alga is rare or not abundant. However, three different metabarcodes were found in the Tara Oceans dataset that exhibited only up to ~90% identity to 18S rRNA sequences in GenBank, and thus could not readily be matched to any known taxon, yet were suggested to be on the same branch as *Olisthodiscus* based on a maximum likelihood-based algorithm for placement of short sequences onto a reference tree (Fig. S2 in the Supporting Information). The details about the abundance and location of respective metabarcodes as well as their sequences are listed in Table S5 in the Supporting Information.

Phylogeny.

The phylogenetic analysis of concatenated 18S and partial 28S rRNA sequences placed *Olisthodiscus* into a deeply diverged branch with the position differing between methods and lacking statistically significant support. In the Bayesian analysis it formed a sister lineage of Pinguiophyceae (Fig. 5), but in the ML analysis of the same dataset was sister to all other ochrophytes except for diatoms and Bolidophyceae (not shown). The *Olisthodiscus* branch was maximally supported and included the two *Olisthodiscus* strains, grouped together with a posterior probability of 1.0 and ML bootstrap support of 99%, along with two nearly identical environmental 18S rDNA clones from uncultured phytoplankton (accession numbers KP404867 and AY180021) forming a closely related sister group of *Olisthodiscus*.

In the tree inferred from a supermatrix (17,531 amino acid positions) of 69 concatenated conserved plastid genome-encoded proteins (Fig. 6A), *Olisthodiscus luteus* K-0444 was placed with strong support (posterior probability 1.0, ML bootstrap value 97%) as a sister lineage to the maximally supported clade Limnista, comprised of Eustigmatophyceae, Chrysophyceae (incl. Synurales), and *Synchroma pusillum* (Synchromophyceae). Since this analysis did not include some ochrophyte classes due to the unavailability of appropriate plastid sequence data, a smaller dataset combining five plastid genome-encoded proteins (*Rbc*L, *Psa*A, *Psb*A, *Psb*C, *Cbb*X) with two plastidial rRNA genes (16S and 23S), and including sequences from all formally described ochrophyte classes, was prepared and analyzed. In the resulting tree (Fig. 6B), *O. luteus*

constituted a sister group of Pinguiophyceae (ML bootstrap value 72%), and the *Olisthodiscus*+Pinguiophyceae clade was sister to Limnista (ML bootstrap value 57%).

Plastid genome.

The plastid genome of *Olisthodiscus luteus* K-0444 is a conventional circular-mapping molecule 155,916 bp long, with two inverted repeats (31,049 bp) separated by the large (83,199 bp) and small (10,619 bp) single-copy region (Fig. 7). The annotated genes include (ignoring duplications in inverted repeats) 141 standard plastid protein-coding genes, one ORF lacking discernible homologs in other plastid genomes, 28 tRNA genes, genes for the three standard rRNAs (5S, 16S, 23S), and the *ssrA* gene specifying tmRNA (Table S2). The set of protein-coding genes is notable for the presence of two genes that are rare in the previously sequenced ochrophyte plastid genomes: *rpoZ*, encoding the omega subunit of RNA polymerase, and *cemA*, encoding a protein of unknown function (potential ion transporter) localized to the plastid inner membrane. In addition, the *O. luteus* plastid genome includes three genes that have not been reported from plastid genomes of other ochrophytes: *ycf80* encoding a Tic22 family protein, and *cysT* and *cysW* organized as a two-gene cluster and encoding subunits of a sulfate transporter. The former did not give any significant hits when used as a query in blast searches, but its homology to Tic22 was supported by two different more sensitive homology detection tools. Specifically, HHpred retrieved the Tic22 family (Pfam PF04278) as the best hit with the e-value 0.00071, and Phyre2 matched a part of the protein to the 3D structure of the *Anabaena* Tic22 (c4ev1A) with a confidence of 94.1% (with *Plasmodium* Tic22 being the second best hit). Furthermore, the putative *Olisthodiscus ycf80* is directly adjacent (in the tail-to-tail orientation) to the gene *rps4*, exactly as found for the gene *ycf80* in various red algal plastid genomes (Table S6 in the Supporting Information). Phylogenetic analysis of CysT and CysW protein sequences (combined into a single tree, as they are mutual paralogs) indicated that the *Olisthodiscus* genes are most closely related to their respective homologs encoded by plastid genomes of cyanidiophyte red algae (Fig. S3 in the Supporting Information). The position of the *cysT* and *cysW* genes relative to other genes in the *Olisthodiscus* plastid genome is shared with the cyanidiophytes, except for the loss in *Olisthodiscus* of the gene *crtR* (=*desA*), which in the red algal plastid genomes is immediately downstream of *cysW* (Fig. S4 in the Supporting Information).

Pigments.

Olisthodiscus strains K-0444 (Fig. 8A) and NIES-15 (Fig. 8B) both contained chlorophylls *a*, c_1 and c_2. The major carotenoids detected were fucoxanthin, violaxanthin and zeaxanthin. β-Carotene, antheraxanthin and violaxanthin-like carotenoids were also present.

DISCUSSION

Reassessing the morphology of Olisthodiscus.

There are no doubts that the two strains, K-0444 and NIES-15, investigated in this study represent the genus *Olisthodiscus*, as we detected all morphological features and life cycle stages described and depicted by Carter (1937). Specifically, the variation of cell shape from round to ovate, dorsally convex and ventrally concave body shape along with the prominent dorsoventral flattening, subanterior or nearly central emergence of two unequal flagella from the ventral depression close to the nucleus, swimming without rotation, presence of multiple rounded or elliptical parietal plastids in vegetative cells, reproduction by longitudinal fission, cyst formation, and presence of conspicuous appendages ("pseudopodia" and crenate cell coating) were all found in accordance with Carter's account on *O. luteus*. The lack of eyespots and contractile vacuoles was also confirmed. *Olisthodiscus* was described as missing pyrenoids, but Carter (1937) noted the presence of unrecognized bodies internal to the plastids, which later were shown to be protruding pyrenoids in NIES-15 (Hara et al. 1985). We detected the same type of pyrenoids in the strain K-0444 as well (Figs. 1B and 3A). The nucleus in both strains was found to be either central or anterior, but it can slightly migrate before cell division, making its position unstable. The most outstanding finding was the presence of the prominent extraplastidial globule occurring in some cells of both strains. Carter (1937) also noted small red or brown globules in the cells of *O. luteus*, which she considered food vacuoles. However, the size and texture of globules observed in K-0444 and NIES-15 resemble the pigmented lipidic bodies (reddish globule) found in members of the class Eustigmatophyceae (Eliáš et al. 2017) rather than a food vacuole.

In addition, we obtained evidence that the life cycle of *Olisthodiscus* is more complicated than previously considered. Apart from reproduction involving cell division into two daughter cells, zoospores were also detected (Figs 1, V and W, and 4D). They were biflagellate, contained one to two plastids, lacked eyespots and were also covered by scales and stalked protrusions as found in vegetative cells. Zoosporangia contained at least five zoospores (Fig. 1L). Cells with crenate appendages were also commonly encountered in our cultures (Fig. 1T). Carter (1937) considered spherical cells with crenate protuberances as cysts. The similar appearance of cysts

was found, for example, in *Heterosigma akashiwo* (Kim et al. 2015). However, the putative cysts of *Olisthodiscus* did not possess any germination pores or empty wall cases as found in *Heterosigma*. Instead, they seemed to divide forming two daughter cells (Fig. 1U). Some mature vegetative cells were observed to also possess such crenate protuberances, meaning they were formed by the division of cells that had undergone a period of dormancy. Cysts could also represent zygospores; however, we did not observe any direct mating.

The SEM investigation of both strains confirmed that the cell surface of *Olisthodiscus* is covered by scales and fibres (Fig. 2), corresponding to the cell covering observed previously in NIES-15 (Inouye et al. 1992) and herein also detected in K-0444 (Figs 3, A–C, and 4, A–H). Additionally, the SEM uncovered two types of surface protrusions: stalked and non-stalked beads (Fig. 2, G and F). Stalked protrusions appear as elongated beads under the LM (Fig. 1, D and P). This shows that the different *Olisthodiscus* strains have a special cell covering not known in other ochrophytes. The SEM data showed that *Olisthodiscus* does not have a sulcus confining the posterior flagellum, as previously claimed by Cavalier-Smith and Scoble (2013). Our data confirmed that the two flagella indeed arise from a ventral depression as originally described (Carter 1937). A similar flagellar swelling as observed in K-0444 (Fig. 2D) was also found, for example, in the raphidophyte *Heterosigma* and the dictyochophyte *Florenciella* (Engesmo et al. 2016), but whether these are homologous structures in unknown.

Multiple species exist in Olisthodiscus.

Despite the general morphological similarity of the two *Olisthodiscus* strains examined, they show substantial genetic differentiation in all genes that could be compared between them (18S and 28S rRNA, *rbc*L, GapC1, GapC2). This agrees with an observation made previously by Connell (2002), who noticed the only 80% identity of the ITS rDNA region of the K-0444 and NIES-15 strains. Indeed, our detailed comparison of the predicted ITS2 secondary structures revealed numerous indels and substitutions including, critically, four CBCs in helices II and III (Fig. S1). The presence of CBCs correlates in well-studied organisms, including microalgae, with reproductive isolation (i.e., inability of crossing) and is frequently used as a criterion to delimit separate species (Coleman 2009, Leliaert et al. 2014). We, therefore, conclude that the strains K-0444 and NIES-15 should be considered two different species.

Disregarding the smaller cell size, the morphology of K-0444 matched well the original description of *Olisthodiscus luteus* (Fig. 1, A–L). NIES-15 cells were also smaller than previously

measured (Hara et al. 1985), suggesting that culturing conditions and media could slightly alter their morphometrics. Furthermore, additional life cycle stages (e.g., zoospores) were formed. Carter (1937) described *O. luteus* from a shallow water area in the Isle of Wight, UK, and K-0444 originates from the Sound between Denmark and Sweden. The geographic proximity makes it likely that K-0444 represents the same species as the one observed by Carter (1937). NIES-15 was isolated from the Seto Inland Sea in Japan, geographically distant from England, and clearly differs morphologically from *O. luteus* in having more laterally compressed and slightly longer cells. Moreover, several scale layers and double scales were detected in NIES-15 but not observed in K-0444. Most importantly, the scale stacks of both strains were composed of a different number of pentagonal plates, with K-0444 possessing slightly longer scales than the NIES-15.

Notably, the two previously described *Olisthodiscus* species, *O. carterae* and *O. magnus*, do not match the studied isolates, since they both exhibit different cell shapes, lack dorsoventral flattening, have a different orientation and insertion of the flagella, and also have a different number of plastids (Hulburt 1965). Unsurprisingly, *O. carterae* was shown to be conspecific with *Hererosigma akashiwo* and was transferred by Taylor (1992) to *Heterosigma* with the new species combination *H. carterae* having priority over *H. akashiwo*. However, the proposed name change was not accepted because no holotype of *O. carterae* was designated by Hulburt (1965), leaving *H. akashiwo* as the valid name and *O. carterae* as nom. inval. (Hallegraeff and Hara 2003). The globular to cylindrical cell shape, an exceptionally large size, and the lateral apical insertion of flagella in *O. magnus* rule out identifying this species with any of the strains studied here. Thus, the NIES-15 strain is below formally described as a new species, *Olisthodiscus tomasii* sp. nov.

Olisthodiscus *represents an independent, deeply diverged ochrophyte lineage.*

Our phylogenetic analyses demonstrate that *Olisthodiscus* is not a member of the Raphidophyceae (see also Fig. S5 in the Supporting Information, which presents a phylogenetic analysis of the 18S rRNA gene including all Raphidophyceae species represented in the GenBank database) and suggest that it represents a lineage of its own, deeply separated from other known ochrophyte groups. Whereas 18S rRNA alone or its combination with partial 28S rRNA sequences data does not confer enough phylogenetic signal to resolve the relationships among the main groups of the Ochrophyta and to place the *Olisthodiscus* lineage with confidence, the phylogenomic analysis of the large datasets based on plastid proteins did yield a tree with high support values even for the deepest branches (Fig. 6A). Our results are congruent with outcomes of similar analyses reported

before (Ševčíková et al. 2015, Han et al. 2019, Kim et al. 2019,) and support the existence of three primary clades of ochrophytes initially proposed on the bases of a five-gene analysis carried out by Yang et al. (2012) and referred to as SI to SIII. We confirm the circumscription of the clade SI, which comprises the PX clade (Phaeophyceae, Xanthophyceae and a series of smaller classes closely related to them) plus Raphidophyceae, and of the clade SIII, which includes Bacillariophyceae (sensu lato, i.e., all diatoms), Bolidophyceae, Pelagophyceae, and Dictyochophyceae. However, employing the first multigene analysis that includes *Olisthodiscus* and a member of Synchromophyceae (*Synchroma pusillum*), our study sheds new light onto the concept of the clade SII.

Firstly, synchromophytes are recovered in a sister position to Chrysophyceae (including Synurales), as expected based on previous analyses of much smaller sequence datasets (Yang et al. 2012). The addition of *Synchroma* (by using plastid gene sequences extracted from a publicly available transcriptome assembly) is important in that it breaks the long stem branch of chrysophytes, which in theory should decrease the impact of the so-called long branch-attraction (LBA) artefact on placing chrysophytes with respect to other groups with long branches in the tree. Hence, the fact that the addition of *Synchroma* to the analysis does not diminish support for the branch uniting chrysophytes (and synchromophytes) with Eustigmatophyceae (that are also characterized by a long stem) reinforces the notion that this grouping, sometimes called Limnista (Ševčíková et al. 2015), is real and not a result of artefactual attraction of rapidly evolving plastid gene sequences from chrysophytes and eustigmatophytes in phylogenies.

Secondly, since our plastid phylogenomics places *Olisthodiscus* with strong support as a sister lineage of Limnista (Fig. 6A), we suggest that the SII clade needs to be expanded to include the *Olisthodiscus* lineage in addition to its original constituents (i.e., classes of the Limnista clade plus Pinguiophyceae; the latter class not represented in our 69 gene-based tree due to lack of data). The relative branching order of Limnista, Pinguiophyceae, and *Olisthodiscus* within the SII clade cannot be robustly established, but our 7-gene phylogeny suggests with moderate support that Pinguiophyceae and *Olisthodiscus* are deeply diverged sister lineages (Fig. 6B). Interestingly, the sister relationship of Pinguiophyceae and the *Olisthodiscus* lineage is suggested by our Bayesian analysis of the combined 18S and 28S rRNA genes, although without any statistical support (Fig. 5). Obviously, this relationship needs to be tested further, ideally by employing independent sets of phylogenetic markers, such as multiple proteins encoded by nuclear or mitochondrial genomes. Interestingly, the unity of the Limnista and the whole clade SII has been challenged by a

phylogenomic analysis (Noguchi et al. 2016). Their tree inferred from a large dataset comprised of 245 nucleus-encoded proteins did not retrieve the monophyly of the clade SII, as the single eustigmatophyte included (*Nannochloropsis gaditana*) branched sister to clade I, while Pinguiophyceae and Chrysophyceae did cluster together, but with poor support. It will be interesting to see how the results of such an analysis changes when the sampling is improved by adding data from *Olisthodiscus* and additional eustigmatophytes.

The plastid genome of Olisthodiscus luteus *reveals novel aspects of plastid genome evolution in ochrophytes.*

The complement of plastid genes reinforces the independent position of *Olisthodiscus* in ochrophytes (Table S2). For example, it includes 13 genes (disregarding the single non-conserved ORF) that are missing from members of Dictyochophyceae and Pelagophyceae. In further contrast to dictyocho- and pelagophytes, but, similar to members of some other ochrophyte groups (the PX clade, Eustigmatophyceae, Synurales; Ševčíková et al. 2015, Kim et al. 2019), *Olisthodiscus* harbours a conserved ancestral intron in the *trnL(UAA)* gene. These observations provide further evidence that placing *Olisthodiscus* with dictyochophytes and pelagophytes into a single class, Hypogyristea, on the basis of a weakly supported 18S rRNA tree topology (Cavalier-Smith and Scoble 2013) was premature. Unfortunately, no plastid genome sequences are available for pinguiophytes, which is the possible closest group to *Olisthodiscus* based on our phylogenetic analysis of seven plastid genes (Fig. 6B). We cannot currently ascertain how this presumed specific relationship manifests in the degree of similarity in the plastid genes.

Sequencing the *Olisthodiscus luteus* K-0444 plastid genome also uncovered some features that illuminate plastid genome evolution in ochrophytes in general. Firstly, *O. luteus* is only the third ochrophyte reported to have the gene *rpoZ* (also called *ycf61*) encoding the omega subunit of the plastidial RNA polymerase; the other two species are the bolidophyte *Triparma laevis* (Tajima et al. 2019) and the dictyochophyte *Florenciella parvula* (Han et al. 2019). The gene is short and poorly conserved, so we reasoned that it may be more common in ochrophyte plastid genomes but overlooked. To test this, we created a profile hidden Markov model (hmm) from an alignment of the three ochrophyte RpoZ proteins and used HMMER (Eddy 2011) to search all potential proteins and peptides (≥50 amino acids) obtained by conceptual translations of various ochrophyte plastid genomes. No significant hit was found (apart the three genomes known to have the gene), in contrast to the positive control of a red algal plastid genome with an annotated *rpoZ* gene

(results not shown). Hence, *rpoZ* is truly rare in ochrophytes, raising the question of the origin of the three instances mentioned above. Han et al. (2019) considered two possibilities, either independent acquisition of *rpoZ* by HGT in the *T. laevis* and *F. parvula* lineages, or multiple loss among ochrophytes. With the discovery of a third *rpoZ*-bearing ochrophyte, which is distantly related to the two previously known ones, the odds seem to be in favor of the presence of *rpoZ* in the plastid genome of the common ochrophyte ancestor, followed by multiple independent loss events.

The second notable gene found in the *Olisthodiscus luteus* plastid genome is *cemA* (also called *ycf10*), encoding a poorly characterized protein located in the inner plastid envelope and proposed to function as an H^+ transporter (Sasaki et al. 1993, Harada et al. 2019). Although common in plastid genomes of Chloroplastida, red algae and cryptophytes, the gene was unknown from ochrophytes until its recent discovery in the plastid genomes of synuralean chrysophytes by Kim et al. (2019). The authors carried out a phylogenetic analysis of CemA proteins, which showed the synuralean CemA sequences branching with strong support within homologs from Chloroplastida, specifically sister to sequences from a subset of Streptophyta. This led to a hypothesis that the *cemA* gene was transferred horizontally from a green algal donor to the plastid genome of the Synurales ancestor (Kim et al. 2019). With the identification of *cemA* in *O. luteus* we revisited this idea. Intriguingly, we also found a *cemA* homolog in the publicly available transcriptome assembly from *Synchroma pusillum* (i.e., a representative of one more ochrophyte lineage; Synchromophyceae). The transcript (MMETSP1452-TRINITY_DN6859_c0_g1_i1; Johnson et al. 2019) is clearly derived from the plastid genome, owing to the fact it includes coding sequences of other typical plastid genes (*ftsH*, *ilvB*). We added the two newly identified ochrophyte CemA sequences to the alignment employed by Kim et al. (2019) and inferred a tree, which no longer showed the synuralean sequences as related to green algal and plant homologs. Instead, they joined the CemA sequences from *O. luteus* and *S. pusillum*, creating a single ochrophyte clade that branched outside the radiation of sequences from Chloroplastida (Fig. S6 in the Supporting Information). Thus, the clustering of the extremely divergent CemA sequences from Synurales and streptophytes in the tree reported by Kim et al. (2019) most likely resulted from an LBA artefact, which was alleviated by the addition of the much less divergent CemA sequences from *O. luteus* and *S. pusillum*. Vertical inheritance from a red algal ancestor rather than HGT is additionally supported by the fact that the *cemA* gene in *O. luteus* (Fig. 7) and Synurales (fig. 1 in Kim et al. 2019) is placed in the tail-to-tail orientation next to the gene *psa*L,

which is an arrangement conserved in at least some cryptophytes (e.g., *Guillardia theta*; accession number NC_000926.1) as well as rhodophytes (e.g., *Galdieria sulphuraria*; accession number NC_024665.1). Hence, we propose that like *rpoZ*, *cemA* was present in the plastid genome of the ochrophyte common ancestor and lost multiple times in different ochrophyte lineages, rather than acquired by HGT from a green algal source.

The most striking attribute of the *Olisthodiscus luteus* plastid genome is the presence of three genes never before reported from other ochrophyte plastid genomes. One is a divergent homolog of *ycf80*, a gene previously documented in plastid genomes of red algae and haptophytes and proposed to encode Tic22, a subunit of the plastid protein translocon (Hovde et al. 2014). The existence of a Tic22-encoding gene in a red algal plastid genome has already been reported without any details (Reumann et al. 2005), but was contested by other authors (Kalanon and McFadden 2008). Hovde et al. (2014) did not provide any specific evidence for their claim. We revisited the identity of the rhodophyte and haptophyte *ycf80* products by employing HHpred searches, which yielded unambiguous statistical support for the homology to Tic22 (Table S6). Furthermore, we show that the *ycf80* gene is also present in plastid genomes of cryptophytes, where it is clustered with the *rps4* gene in the same way as found in many red algal and *Olisthodiscus* plastid genomes (Table S6). Hence, the *ycf80* gene is widely distributed in plastids of red algae and their evolutionary descendants, but why it was lost by plastid genomes of most ochrophytes (except *Olisthodiscus*) remains to be investigated.

The other two genes novel for an ochrophyte plastid genome are *cysT* and *cysW*. An earlier analysis indicated limited distribution of these genes in plastid genomes, with *cysT* found in green algae, a liverwort, and the rhodophyte *Cyanidioschyzon merolae*, whereas *cysW* was reported only from the latter red alga (Ohta et al. 2003). Except for the identification of both genes in *Olisthodiscus*, the presently available sequence data are consistent with the previous insight (Fig. S3). We found plastidial *cysW* only in a single rhodophyte lineage, Cyanidiophyceae, including *C. merolae* and its relatives (*Galdieria sulphuraria* and an unidentified representative referred to as Cyanidiaceae sp. MX-AZ01). Cyanidiophytes also possess *cysT*, which is additionally found only in green algae and bryophytes (sensu lato). The results of our phylogenetic analysis (Fig. S3) and the position of the *cysT* and *cysW* genes in the *Olisthodiscus* plastid genome being conserved with those seen in cyanidiophytes (Fig. S4), provide strong evidence that these two genes were passed vertically from a red algal ancestor of the *Olisthodiscus* plastid. Given phylogenetic evidence for the common ancestry of plastids in all ochrophytes, haptophytes, cryptophytes and the Myzozoa

subgroup of Alevolata, i.e. "chromalveolates" (Ševčíková et al. 2015, Muñoz-Gómez et al. 2017), all these groups, except *Olisthodiscus*, must lack *cysT* and *cysW* as a result of multiple losses. Furthermore, since the red algal ancestor of the "chromalveolate" plastids belonged to a lineage that branched off in the red algal phylogeny only after the divergence of Cyanidiophyceae (Muñoz-Gómez et al. 2017), *cysT* and *cysW* were most likely lost only before the radiation of the "core" rhodophytes (i.e., subphyla Proteorhodophytina and Eurhodophytina).

The presence of the *cysT* and *cysW* in the *Olisthodiscus* plastid genome is interesting also from afunctional viewpoint, as it implies the presence of a particular type of a molecular machinery mediating sulfate import into the *Olisthodiscus* plastid. Studies in bacteria showed the existence of a multisubunit sulfate (or thiosulfate) permease, SulT that consists of the CysT/CysW pair of transmembrane proteins constituting a membrane channel, the ATP-binding protein CysA bound to CysT/CysW from the cytosolic side and coupling ATP hydrolysis to the translocation of sulfate, and a periplasmic protein binding the substrate, specifically Sbp specific for sulfate or CysP specific for thiosulfate (Aguilar-Barajas et al. 2011). Interestingly, we identified transcripts encoding homologs of CysA and Sbp, but not CysP, in our unpublished transcriptome assembly from *O. luteus* K-0444, and both are specifically related to their respective homologs encoded by nuclear genomes of Cyanidiophyceae (Figs. S7 and S8 in the Supporting Information). Hence, *Olisthodiscus* is apparently capable of assembling a functional SulT permease importing sulfate into its plastid, and it inherited the whole machinery from red algae, presumably via endosymbiotic gene transfer in case of CysA and Sbp. We did not find any homologs of CysA, Sbp, or CysP in available genomic and transcriptomic data from other ochrophytes or other groups with a red alga-derived secondary plastid (haptophytes, cryptophytes, myzozonas). Based on this we predict that no *cysT* and *cysW* genes will be found in plastid genomes in hitherto unstudied ochrophyte taxa, including the potential *Olisthodiscus* sister group, pinguiophytes. Why *Olisthodiscus* so uniquely among all these taxa keeps the SulT permease is a question that needs to be addressed.

Olisthodiscus *typifies a new class of ochrophyte algae.*

The isolated phylogenetic position of *Olisthodiscus* evident from molecular phylogenetic analyses and attributes of its plastid genome is reflected also by its uniqueness at the phenotypic level, including the ultrastructure and pigment composition. Earlier comparative analyses of the ultrastructure of the NIES-15 strain (Hara et al. 1985, Inouye et al. 1992) did not allow its

assignment to any ochrophyte group known at the time. Since then, two novel groups of ochrophytes have been discovered that need to be compared with *Olisthodiscus*: *Sulcochrysis biplastida* (Honda et al. 1995) and the class Pinguiophyceae (Kawachi et al. 2002).

The former was proposed to be related to *Olisthodiscus* by Cavalier-Smith and Scoble (2013), but on closer inspection these algae seem to have few specific characters in common (Hara et al. 1985, Inouye et al. 1992, Honda et al. 1995). Above all, *Sulcochrysis* possesses a sulcus (a distinct groove) extending longitudinally and reaching the posterior cell end, where the short posterior flagellum is embedded, whereas *Olisthodiscus* clearly lacks such a prominent structure. A proximal (=transitional) helix with two gyres located below the transitional plate in the flagellar transitional region was found in *Sulcochrysis*, whereas in *Olisthodiscus* the transitional helix is absent. In further contrast to *Sulcochrysis*, *Olisthodiscus* contains a rhizoplast (a system II fiber) and a structure termed the proximal plate, with a conspicuous sigmoid edge, linking the flagellar basal bodies to the nucleus. In *Sulcochrysis*, basal bodies are situated in the nuclear depression. Microtubular roots R1, R2, R3, R4 are composed of 15, 1, 5 and 2 microtubules, respectively, in *Olisthodiscus*, and 2, 1, 6 and 2 in *Sulcochrysis*. In addition, R3 and R4 extend posteriorly parallel to each other along the opposite sides of the sulcus, a unique feature of *Sulcochrysis* not found in *Olisthodiscus*. Moreover, the extra microtubule extending posteriorly along the R3 root was found in *Sulcochrysis biplastida*, and two microtubules of the R3 root form a coil that is located on the Golgi body in *Sulcochrysis*, whereas R3 coiling is absent in *Olisthodiscus*. Finally, *Olisthodiscus* is obligately autotrophic, while *S. biplastida* is mixotrophic with a food vacuole in the posterior cell end.

Careful ultrastructural comparison of *Olisthodiscus* and pinguiophytes is motivated by our phylogenetic analyses suggesting a specific relationship between these two taxa. However, such a comparison is not straightforward, since pinguiophytes themselves do not have unifying ultrastructural features (Kawachi et al. 2002). They encompass both motile (*Glossomastix*, *Phaeomonas* and *Polypodochrysis*) and non-motile (*Pinguiochrysis* and *Pinguiococcus*) taxa, with typical stramenopile-like or unique flagellar arrangements. Similarities among *Olisthodiscus* and pinguiophytes include, for instance, the presence of the rhizoplast (in all flagellate species) and additional cytoskeletal microtubules extending toward the cell posterior (in *Polypodochrysis*). As in *Olisthodiscus*, membranes penetrate into the pyrenoid in all five pinguiophyte species. As in *Olisthodiscus*, no mixotrophy and food vacuoles were found in pinguiophytes. On the other hand,

the transitional helix with two or three gyres and an extra microtubule (designated as the bypassing root) are present in pinguiophytes and missing in *Olisthodiscus*.

Apart from the detailed visualization of the scales covering the *Olisthodiscus* cell surface (not found in Raphidophyceae, Pinguiophyceae and *Sulcochrysis*), a noteworthy TEM observation was the re-detection of peripheral vesicles lying between the plasmalemma and plastids. They were previously termed as "a thin cytoplasmic periplast" by Hara et al. (1985). The term periplast is used for the specific and well-defined cell covering of Cryptophyceae, and we therefore prefer peripheral vesicles for *Olisthodiscus*. The membranous structures underlying the plasmalemma (Figs. 3, A and C, and 4G) likely develop into the peripheral vesicles, whose fundamental function may be to keep the protoplast firm but flexible. The peripheral vesicles seem to enclose most of the protoplast and have a row of underlying microtubules. Despite such vesicles being a rare ultrastructural feature among ochrophytes, similar structures were observed in the raphidophyte *Heterosigma akashiwo* (Ishida et al. 2000) and a non-photosynthetic stramenopile relative of ochrophytes, the flagellate *Developayella elegans* (Tong 1995). They were termed "vacuole-like vesicles" and "cortical vesicles", respectively. The system of peripheral vesicles in *Olisthodiscus* is also reminiscent of the cell covering in dinoflagellates (Leadbeater and Green 1993), the amphiesma, which is a system of flattened vesicles underlying the plasmalemma, with individual or grouped microtubules beneath. The amphiesma is regarded as a homolog to the cortical alveoli of other alveolates, a group of protists related to the stramenopiles within the supergroup SAR (Adl et al. 2012). Whether the peripheral vesicles of *Olisthodiscus* are homologous to any of the similar structures observed in other stramenopiles or more distantly related organisms, or whether they resulted from convergent evolution cannot be answered without knowing the molecular basis of their formation.

The observed pigment pattern of the two *Olisthodiscus* strains examined (K-0444 and NIES-15), with the presence of chlorophylls c_1 and c_2, and fucoxanthin, violaxanthin and zeaxanthin as major carotenoids, resembles the predominant pigment pattern found in chrysophytes (Jeffrey et al. 2011). The presence of antheraxanthin as a minor pigment also matches the pattern of chrysophytes, but the high peak of the pigment "Chl c_2-*Pavlova gyrans*" present in chrysophytes (Jeffrey et al. 2011) was missing in *Olisthodiscus*. The most similar pigment patterns reported in the literature are those from *Heterosigma akashiwo* (Okumura et al. 2001, Rodriguez et al. 2006) and, of course, the NIES-15 strain (i.e., *O. tomasii*; Mostaert et al. 1998), where only the presence of auroxanthin-like pigment differs from our analysis. The

auroxanthin is a pigment produced by the degradation of violaxanthin, and it is possible that the previous treatment (freeze-drying) of the cells by Mostaert et al. (1998) could have effects in the degradation of pigments, as they suggested. Among other groups, the pinguiophytes do not have antheraxanthin, and the proportions of violaxanthin and zeaxanthin related to fucoxanthin are lesser than those observed in the *Olisthodiscus* strains examined in the present study (Kawachi et al. 2002). These three groups (chrysophytes, pinguiophytes and raphidophytes) share the presence of chlorophylls c_1 and/or c_2, fucoxanthin, violaxanthin, zeaxanthin and β-carotene, and are the closest groups to *Olisthodiscus* based on pigment composition, which is consistent with the phylogenetic position of *Olisthodiscus* as indicated by our plastid phylogenomic analysis. Other ochrophyte groups, such as diatoms, as well as dictyochophytes and pelagophytes, seem more distantly related, containing chlorophyll c_3, fucoxanthin derivatives and diadinoxanthin, and sometimes lacking violaxanthin.

Altogether, the unique combination of cytological and biochemical features of *Olisthodiscus*, together with the robust support for it representing a phylogenetic lineage deeply separated from all formally described ochrophyte classes, indicate that *Olisthodiscus* needs to be placed into a separate class as its sole currently confirmed constituent genus. Two environmental nearly complete 18S rRNA sequences from uncultured organisms, the "uncultured eukaryote clone WS073.126" from the South China Sea (Wu et al. 2015) and the "uncultured stramenopile clone CCW34" isolated from an oxygen depleted water column at Cape Cod (Stoeck and Epstein 2003), are closely related to *Olisthodiscus* (Fig. 5), revealing the existence of a broader phylogenetic diversity within this lineage (another species or possibly a separate genus). The existence of additional organisms, more deeply diverged from *Olisthodiscus* yet potentially more closely related to it than to any other ochrophyte lineage known, is suggested by our analysis of metabarcoding data from marine localities (Fig. S2). Although more complete sequence data are needed to corroborate this suggested relationship, it is likely that the *Olisthodiscus* clade might be significantly more diverse than could be inferred from cultured organisms.

The possible specific relationship of *Olisthodiscus* and *Sulcochrysis biplastida*, hypothesized by Cavalier-Smith and Scoble (2013) cannot be directly tested lacking DNA sequence data (and inaccessibility of a culture) for the latter species. Based on morphology and ultrastructure, Honda et al. (1995) considered *S. biplastida* not to be assignable to any ochrophyte group, but pointed to certain similarities of its flagellar apparatus to those of dichtyochophytes and pelagophytes. Interestingly, in a later study, Honda and Inouye (2002, p. 85) mentioned as their

unpublished result that "*Sulcochrysis* often forms a clade with the Dictyochophyceae in 18S rDNA analyses that is supported by high bootstrap values". More recently, Honda et al. (2007, p. 82) stated of *S. biplastida* that "...based on an 18S rRNA gene phylogeny, [it] should be classified in the Dictyochophyceae (Honda et al. unpubl. data)". *Olisthodiscus* and *Sulcochrysis* indeed have little in common at the morphological and ultrastructural level (see above). Most likely they are not closely related, and there is no reason to place *Sulcochrysis* in the same class as *Olisthodiscus*.

As mentioned in the Introduction, the separate class "Olisthophyceae" proposed for *Olisthodiscus* as early as in 1999 in a thesis (Tyrrell 1999) was not effectively published. Validly published taxa specifically accommodating *Olisthodiscus* include the family Olisthodiscaceae, the order Olisthodiscales, and the subclass Sulcophycidae, all established by Cavalier-Smith (in Cavalier-Smith and Scoble 2003). To assign *Olisthodiscus* to a class, Sulcophycidae could be elevated to the class rank (i.e., "Sulcophyceae"). However, we object to such a treatment for several reasons. (1) The name would imply the presence of a *sulcus* (groove) in the members of the class, but our investigations did not confirm it in either of the two *Olisthodiscus* species. (2) The diagnosis of the subclass also stated the cells to be "naked" and exhibiting "two indistinct stacked dense rings below the flagellar transition zone dense plate". The former is not true for *Olisthodiscus* and the latter is found in *Sulcochrysis*, but not in *Olisthodiscus*. (3) The diagnosis explicitly states the absence of "cortical alveoli", but potentially homologous structures, here referred to as peripheral vesicles, are present in *Olisthodiscus*. (4) Finally, the name would elicit connotations to *Sulcochrysis*, which most likely does not belong to the class accommodating *Olisthodiscus*. The most appropriate solution, in our view, is to erect a new class, Olisthodiscophyceae, with a new description taking into account the new findings on *Olisthodiscus* gathered in this and previous studies.

Ochrophyta Cavalier-Smith 1995

Olisthodiscophyceae Barcytė, Eikrem & M.Eliáš, classis nov.

Typified name derived from the genus name *Olisthodiscus* N.Carter

Description: Cells ellipsoidal to spherical and dorso-ventrally flattened with shallow depression on the ventral side. One side concave and the other convex. Heterokont flagella emerging from the concave side, anterior flagellum with hairs, posterior flagellum smooth. Cell surface covered by scales. One nucleus and numerous plastids surrounded by four membranes, the outermost being continuous with the endoplasmic reticulum; with girdle lamella. Plastids with chlorophylls *a, c1*

and *c2*, and xanthophylls fucoxanthin, zeaxanthin, antehraxanthin, and violaxanthin. Peripheral vesicles present beneath the plasmalemma. Extrusomes absent. Asexual reproduction by longitudinal fission and zoospores; sexual reproduction unknown, cysts produced. Present in brackish/marine waters. Forms a distinct phylogenetic lineage in Ochrophyta deeply diverged from other known classes. Several genes (*ycf80*, *cysT* and *cysW*) retained in the plastid genome uniquely among ochrophytes.
Type species: *Olisthodiscus luteus* N.Carter 1937.

Olisthodiscales Cavalier-Smith emed. Barcytė, Eikrem & M.Eliáš
With the characters of the class.

Olisthodiscaceae Cavalier-Smith emend. Barcytė, Eikrem & M.Eliáš
With the characters of the class.

Olisthodiscus **N.Carter 1937 emend. Barcytė, Eikrem & M.Eliáš**
Emended description: Unicellular organism. Vegetative cells ellipsoidal, ovate, pyriform or round; dorsally convex and ventrally concave; flattened. Protoplast firm with peripheral vesicles underlaying plasmalemma and covered with scales, fibrils and bead-like protrusions. Two unequal flagella emerging anteriorly or nearly centrally from a ventral funnel-shaped depression. Anterior flagellum 1¼–1½ times the cell length and directed forward in motion, with hairs; the smooth posterior flagellum equal in length to the cell or shorter, and trails behind; cells do not rotate while swimming. Multiple parietal plastids with inwardly protruding pyrenoids that are penetrated by plastid membranes. Nucleus central or anterior. Contractile vacuoles and eyespot absent. Extraplastidial coloured globules may be present. Reproduction by longitudinal fission and zoospores. Cysts are formed.
Type species: *Olisthodiscus luteus* N.Carter 1937, *Arch. Protistenkn.* 90: 19.
Lectotype specimen designated here: illustration of a single cell in plate 3, fig. 29 in Carter (1937).

Olisthodiscus tomasii **Barcytė, Eikrem & M.Eliáš, sp. nov.**
Description: Cells ellipsoidal, oval to spherical; dorsally convex and ventrally concave, flattened; covered with scales composed of a stack of five or six subunits and embedded in a mesh of fibrils.

Bead-like protrusions can be seen under the light microscope. Anterior flagellum 1¼–1½ times the cell length and projects forward, with hairs; posterior flagellum around the cell's length; smooth and trails behind; both emerging from a ventral funnel-shaped depression. Vegetative ellipsoidal cells 9-16 µm long and 5-10 µm wide, spherical up to 25 µm in diameter. Cells with 5–13 parietal rounded or elliptical plastids with irregular margins. Pyrenoids penetrated by plastid membranes. Peripheral vesicles present between plasmalemma and plastids. One to two red extraplastidial globules may be present. Nucleus central or anterior. Asexual reproduction by longitudinal cell division and zoospores. Zoospores 7-9 µm long and 4–5 µm wide, biflagellate, and contain one or two plastids. Sexual reproduction not observed. Cysts with crenate protuberances are formed. Morphologically differs from *O. luteus* in cells being more laterally compressed and slightly longer, and in the red extraplastidial globule being considerably larger. Nuclear 18S-ITS1-5.8S-ITS2-28S sequence (KP780272) distinctive.

Holotype: O A-10012. Plastic embedding of strain NIES-15, deposited at the Natural History Museum, University of Oslo, Norway.

Type locality: Seto Inland Sea, Tamano, Okayama, Japan.

Etymology: The species is named in honour of Prof. Carmelo R. Tomas, for his significant contribution to the studies of *Olisthodiscus* and other marine flagellates.

Habitat: marine.

Culture availability: NIES-15, National Institute for Environmental Studies (NIES), Tsukuba, Ibaraki, Japan.

ACKNOWLEDGEMENTS

We thank Kim Jong Im (Chungnam National University, South Korea) for providing a multiple alignment of CemA protein sequences, two anonymous reviewers and Paul W. Gabrielson for their critical and constructive comments on the manuscript, and John McNeill for comments on Latin nomenclature. This work was supported by CePaViP (CZ.02.1.01/0.0/0.0/16_019/0000759) provided by ERD Funds, the Czech Science Foundation grant (18-13458S) to M.E., and the Norwegian Research Council funding the grant 196702/E40 Toxic Algae to AE and WE. We acknowledge Imaging Methods Core Facility at BIOCEV, an institution supported by the MEYS CR (Large RI Project LM2018129 Czech-BioImaging) and ERDF (project No. CZ.02.1.01/0.0/0.0/16_013/0001775) for their support with obtaining some imaging data

presented in this paper. Imaging was also carried out at the Electron Microscopy Facility, Department of Biosciences, University of Oslo. We also thank
John Cawley for proofreading the manuscript and correcting the English.

REFERENCES

Adl, S. M., Simpson, A. G., Lane, C. E., Lukeš, J., Bass, D., Bowser, S. S., Brown, M. W., Burki, F., Dunthorn, M., Hampl, V., Heiss, A., Hoppenrath, M., Lara, E., Le Gall, L., Lynn, D. H., McManus, H., Mitchell, E. A., Mozley-Stanridge, S. E., Parfrey, L. W., Pawlowski, J., Rueckert, S., Shadwick, L., Schoch, C. L., Smirnov, A. & Spiegel, F. W. 2012. The revised classification of eukaryotes. *J Eukaryot. Microbiol.* 59: 429–93.

Aguilar-Barajas, E., Díaz-Pérez, C., Ramírez-Díaz, M. I., Riveros-Rosas, H. & Cervantes, C. 2011. Bacterial transport of sulfate, molybdate, and related oxyanions. *Biometals* 24:687–707.

Altschul, S. F., Madden, T. L., Schäffer, A. A., Zhang, J., Zhang, Z., Miller, W. & Lipman, D. J. 1997. Gapped BLAST and PSI-BLAST: a new generation of protein database search programs. *Nucleic Acids Res*. 25: 3389–402.

Andersen, R. A. Biology and systematics of heterokont and haptophyte algae. 2004. *Am. J. Bot.* 91:1508–22.

Andersen, R. A. 2005. *Algal Culturing Techniques*. 1st ed. Academic Press, Amsterdam, Netherlands, 596 pp.

Bankevich, A., Nurk, S., Antipov, D., Gurevich, A. A., Dvorkin, M., Kulikov, A. S., Lesin, V. M., Nikolenko, S. I., Pham, S., Prjibelski, A. D., Pyshkin, A. V., Sirotkin, A. V., Vyahhi, N., Tesler, G., Alekseyev, M. A. & Pevzner, P. A. 2012. SPAdes: a new genome assembly algorithm and its applications to single-cell sequencing. *J. Comput. Biol.* 19:455–77.

Bellaousov, S., Reuter, J. S., Seetin, M. G., Mathews & D. H. 2013. RNAstructure: Web servers for RNA secondary structure prediction and analysis. *Nucleic Acids Res*. 41:W471–4.

Berger, S. A., Krompass, D. & Stamatakis, A. 2011. Performance, accuracy, and Web server for evolutionary placement of short sequence reads under maximum likelihood. *Syst. Biol.* 60:291–302.

Boczar, B. A., Delaney, T. P. & Cattolico, R. A. 1989. Gene for the ribulose-1,5-bisphosphate carboxylase small subunit protein of the marine chromophyte *Olisthodiscus luteus* is similar to that of a chemoautotrophic bacterium. *Proc. Natl. Acad. Sci. USA* 86:4996–9.

Bolger, A. M., Lohse, M., & Usadel, B. 2014. Trimmomatic: A flexible trimmer for Illumina Sequence Data. *Bioinformatics* 30:2114–20.

Bowers, H. A., Tomas, C., Tengs, T., Kempton, J. W., Lewitus, A. J. & Oldach, D. W. 2006. Raphidophyceae [Chadefaud ex Silva] systematics and rapid identification: sequence analyses and real-time PCR assays. *J. Phycol.* 42:1333–48.

Brown, J. W. & Sorhannus, U. A. 2010. A molecular genetic timescale for the diversification of autotrophic stramenopiles (Ochrophyta): substantive underestimation of putative fossil ages. *PLoS ONE* 5:e12759.

Capella-Gutiérrez, S., Silla-Martínez, J. M. & Gabaldón, T. 2009. trimAl: a tool for automated alignment trimming in large-scale phylogenetic analyses. *Bioinformatics* 25:1972–73.

Carter, N. 1937. New or interesting algae from brackish water. *Arch. Protistenk.* 90:1–68.

Cavalier-Smith, T. & Scoble, J. M. 2013. Phylogeny of Heterokonta: *Incisomonas marina*, a uniciliate gliding opalozoan related to *Solenicola* (Nanomonadea), and evidence that Actinophryida evolved from raphidophytes. *Eur. J. Protistol.* 49:328–53.

Christensen, T. 1980. *Algae: A taxonomic survey. Fasc. 1.* AiO Tryk as, Odense, 216 pp.

Christensen, T. 1994. *Algae: A taxonomic survey. Fasc. 2.* AiO Tryk as, Odense, 256 pp.

Coleman, A. W. 2011. Is there a molecular key to the level of "biological species" in eukaryotes? *Mol. Phylogenet. Evol.* 50:197–203.

Connell, L. B. 2000. Nuclear ITS region of the alga *Heterosigma akashiwo* (Chromophyta: Raphidophyceae) is identical in isolates from Atlantic and Pacific basins. *Mar. Biol.* 136:953–60.

Connell, L. 2002. Rapid identification of marine algae (Raphidophyceae) using three-primer PCR amplification of nuclear internal transcribed spacer (ITS) regions from fresh and archived material. *Phycologia* 41:15–21.

de Vargas, C., Audic, S., Henry, N., Decelle, J., Mahé, F., Logares, R., Lara, E., Berney, C., Le Bescot, N., Probert, I., Carmichael, M., Poulain, J., Romac, S., Colin, S., Aury, J.M., Bittner, L., Chaffron, S., Dunthorn, M., Engelen, S., Flegontova, O., Guidi, L., Horák, A., Jaillon, O., Lima-Mendez, G., Lukeš, J., Malviya, S., Morard, R., Mulot, M., Scalco, E., Siano, R., Vincent, F., Zingone, A., Dimier, C., Picheral, M., Searson, S., Kandels-Lewis, S.; Tara Oceans Coordinators, Acinas, S.G., Bork, P., Bowler, C., Gorsky, G., Grimsley, N., Hingamp, P., Iudicone, D., Not, F., Ogata, H., Pesant, S., Raes, J., Sieracki, M. E., Speich, S., Stemmann, L., Sunagawa, S., Weissenbach, J., Wincker, P. & Karsenti, E. 2015. Ocean plankton. Eukaryotic plankton diversity in the sunlit ocean. *Science* 348:1261605.

Delaney, T.P. & Cattolico, R. A. 1989. Chloroplast ribosomal DNA organization in the chromophytic alga *Olisthodiscus luteus*. *Curr. Genet.* 15:221–9.

Delaney, T. P. & Cattolico, R. A. 1991. Sequence and secondary structure of chloroplast 16S rRNA from the chromophyte alga *Olisthodiscus luteus*, as inferred from the gene sequence. *Nucleic Acids Res.* 19:6328.

Derelle, R., López-García, P., Timpano, H. & Moreira, D. 2016. A phylogenomic framework to study the diversity and evolution of Stramenopiles (=Heterokonts). *Mol. Biol. Evol.* 33:2890–98.

Dorrell, R. G., Gile, G., McCallum, G., Méheust, R., Bapteste, E. P., Klinger, C. M., Brillet-Guéguen, L., Freeman, K. D., Richter, D. J. & Bowler, C. 2017. Chimeric origins of ochrophytes and haptophytes revealed through an ancient plastid proteome. *eLife* 6:e23717.

Eddy, S. R. 2011. Accelerated profile HMM searches. *PLoS Comput. Biol*. 7:e1002195.

Engesmo, A., Eikrem, W., Seoane, S., Smith, K., Edvardsen, B., Hofgaard A. & Tomas, C. R. 2016. New insights into the morphology and phylogeny of *Heterosigma akashiwo* (Raphidophyceae), with the description of *Heterosigma minor* sp. nov. *Phycologia* 55:279–94.

Fukuyo, Y., Takano, H., Chihara, M. & Matsuoka, K. 1990. *Red Tide Organisms in Japan: An Illustrated Taxonomic Guide*. Uchida Rokakuho, Tokyo, pp. 1–430.

Gibbs, S. P., Chu, L. L. & Magnussen, C. 1980. Evidence that *Olisthodiscus luteus* is a member of the Chrysophyceae. *Phycologia* 19:173–7.

Greiner, S., Lehwark, P. & Bock, R. 2019. OrganellarGenomeDRAW (OGDRAW) version 1.3.1: expanded toolkit for the graphical visualization of organellar genomes. *Nucleic Acids Res*. 47:W59–64.

Hallegraeff, G. M. & Hara, Y. 2003. Taxonomy of harmful marine raphidophytes. *In* Hallegraeff, G. M., Anderson, D. M. & Cembella, A. D. [Eds.] *Manual of Harmful Marine Microalgae*. UNESCO Publishing, Paris, pp. 511–22.

Han, K. Y., Maciszewski, K., Graf, L., Yang, J. H., Andersen, R. A., Karnkowska, A. & Yoon, H. S. 2019. Dictyochophyceae plastid genomes reveal unusual variability in their organization. *J. Phycol.* 55:116–80.

Hara, Y., Inouye, I. & Chihara, M. 1985. Morphology and ultrastructure of *Olisthodiscus luteus* (Raphidophyceae) with special reference to the taxonomy. *Bot. Mag. Tokyo* 98:251–62.

Harada, K., Arizono, T., Sato, R., Trinh, M. D. L., Hashimoto, A., Kono, M., Tsujii, M., Uozumi, N., Takaichi, S., Masuda, S. 2019. DAY-LENGTH-DEPENDENT DELAYED-GREENING1, the *Arabidopsis* homolog of the cyanobacterial H^+-extrusion protein, is essential for chloroplast pH regulation and optimization of non-photochemical quenching. *Plant Cell Physiol*. 60:2660–71.

Harmanci, A. O., Sharma, G. & Mathews, D. H. 2008. PARTS: probabilistic alignment for RNA joinT secondary structure prediction. *Nucleic Acids Res*. 36:2406–17.

Hohenberg, H., Mannweiler, K. & Müller, M. 1994. High-pressure freezing of cell suspensions in cellulose capillary tubes. *J. Microsc.* 175:34–43.

Honda, D., Kawachi, M. & Inouye, I. 1995. *Sulcochrysis biplastida* gen. et. sp. nov.: Cell structure and absolute configuration of the flagellar apparatus of an enigmatic chromophyte alga. *Phycol. Res.* 43:1–16.

Honda, D. & Inouye I. 2002. Ultrastructure and taxonomy of a marine photosynthetic stramenopile *Phaeomonas parva* gen. et sp. nov. (Pinguiophyceae) with emphasis on the flagellar apparatus architecture. *Phycol. Res.* 50:75–89.

Horn, S., Ehlers, K., Fritzsch, G., Gil-Rodríguez, M. C., Wilhelm, C. & Schnetter, R. 2007. *Synchroma grande* spec. nov. (Synchromophyceae class. nov., Heterokontophyta): an amoeboid marine alga with unique plastid complexes. *Protist* 158:277–93.

Hovde, B. T., Starkenburg, S. R., Hunsperger, H. M., Mercer, L. D., Deodato, C. R, Jha R. K., Chertkov, O., Monnat Jr R. J. & Cattolico R. A. 2014. The mitochondrial and chloroplast genomes of the haptophyte *Chrysochromulina* tobin contain unique repeat structures and gene profiles. *BMC Genom.*15:604.

Hulburt, E. M. 1965. Flagellates from brackish waters in the vicinity of Woods Hole, Massachusetts. *J. Phycol*. 1:87–94.

Iida, K., Takishita, K., Ohshima, K. & Inagaki, Y. 2007. Assessing the monophyly of chlorophyll-c containing plastids by multi-gene phylogenies under the unlinked model conditions. *Mol. Phylogenet. Evol*. 45:227–38.

Inouye, I., Hara, Y & Chihara M. 1992. Further observations on *Olisthodiscus luteus* (Raphidophyceae, Chromophyta): the flagellar apparatus ultrastructure. *Jap. J. Phycol.* 40:333–48.

Ishida, K., Cavalier-Smith, T. & Green, B.R. 2000. Endomembrane structure and the chloroplast protein targeting pathway in *Heterosigma akashiwo* (Raphidophyceae, Chromista). *J. Phycol.* 36:1135–44.

Jeffrey, S. W., Wright, S. W. & Zapata, M. 2011. Microalgal classes and their signature pigments. *In* Roy, S., Llewellyn C., Egeland, E.S. & Johnsen, G. [Eds.] *Phytoplankton Pigments: Characterization, Chemotaxonomy and Applications in Oceanography*. Cambridge University Press, Cambridge, pp. 3–77.

Johnson, L. K., Alexander, H. & Brown, C. T. 2019. Re-assembly, quality evaluation, and annotation of 678 microbial eukaryotic reference transcriptomes. *GigaScience* 8:giy158.

Kai, A., Yoshii, Y., Nakayama, T. & Inouye, I. 2008. Aurearenophyceae *classis nova*, a new class of Heterokontophyta based on a new marine unicellular alga *Aurearena cruciata* gen. et sp. nov. inhabiting sandy beaches. *Protist* 159:435–57.

Kalanon, M. & McFadden, G. I. 2008. The chloroplast protein translocation complexes of *Chlamydomonas reinhardtii*: a bioinformatic comparison of Toc and Tic components in plants, green algae and red algae. *Genetics* 179:95–112.

Kalvari, I., Argasinska, J., Quinones-Olvera, N., Nawrocki E. P., Rivas, E., Eddy S. R., Bateman, A., Finn, R. D. & Petrov, A. I. 2018. Rfam 13.0: shifting to a genome – centric resource for non-coding RNA families. *Nucleic Acids Res*. 46:D335–42.

Kalyaanamoorthy, S., Minh, B. Q., Wong, T. K. F, von Haeseler, A & Jermiin, L. S. 2017. ModelFinder: fast model selection for accurate phylogenetic estimates. *Nat. Methods* 14:587–9.

Katoh, K. & Standley, D. M. 2013. MAFFT Multiple Sequence Alignment Software Version 7: Improvements in performance and usability. *Mol. Biol. Evol.* 30:772–80.

Kawachi, M., Inouye, I., Honda, D., O'Kelly, C. J., Bailey, J. C., Bidigare, R. R. & Andersen, R. A. The Pinguiophyceae *classis nova*, a new class of photosynthetic stramenopiles whose members produce large amounts of omega-3 fatty acids. *Phycol. Res.* 50:31–47.

Keeling, P. J., Burki, F., Wilcox, H. M., et al. 2014. The Marine Microbial Eukaryote Transcriptome Sequencing Project (MMETSP): illuminating the functional diversity of eukaryotic life in the oceans through transcriptome sequencing. *PLoS Biol*. 12:e1001889.

Kelley, L. A., Mezulis, S., Yates, C.M., Wass, M. N. & Sternberg, M. J. 2015. The Phyre2 web portal for protein modeling, prediction and analysis. *Nat. Protoc*. 10:845–58.

Kim, J., Park, B.S., Wang, P., Kim, J.H., Youn, S.H. & Han, M. 2015. Cyst morphology and germination in *Heterosigma akashiwo* (Raphidophyceae). *Phycologia* 54:435–9.

Kim, J. I., Shin, H., Škaloud, P., Jung, J. Yoon, H. S., Archibald J. M. & Shin W. 2019. Comparative plastid genomics of Synurophyceae: inverted repeat dynamics and gene content variation. *BMC Evol. Biol*. 19:20.

Kryvenda, A., Rybalka, N., Wolf, M. & Friedl, T. 2018. Species distinctions among closely related strains of Eustigmatophyceae (Stramenopiles) emphasizing ITS2 sequence-structure data: *Eustigmatos* and *Vischeria*. *Eur. J. Phycol.* 53:471–91.

Kück, P. & Longo, G. C. 2014. FASconCAT-G: extensive functions for multiple sequence alignment preparations concerning phylogenetic studies. *Front. Zool.* 11:81.

Langmead, B. & Salzberg, S. L. 2012. Fast gapped-read alignment with Bowtie 2. *Nat. Methods* 9:357–9.

Lartillot, N., Rodrigue, N., Stubbs, D. & Richer, J. 2013. PhyloBayes MPI: phylogenetic reconstruction with infinite mixtures of profiles in a parallel environment. *Syst. Biol*. 62:611–5.

Leadbeater, B. 1969. A fine structural study of *Olisthodiscus luteus* Carter. *Br. Phycol. J.* 4:3–17.

Leadbeater, B. & Green, J. C. 1993. Cell coverings of microalgae. *In* Berner, T. [Ed.] *Ultrastructure of Microalgae*. CRC Press, Boca Raton, USA, pp. 71–98.

Leliaert, F., Verbruggen, H., Vanormelingen, P., Steen, F., López-Bautista J. M., Zuccarello, G. C. & De Clerck, O. 2014. DNA-based species delimitation in algae. *Eur. J. Phycol.* 49:179–96.

Logares, R., Audic, S., Bass, D., Bittner, L., Boutte, C., Christen, R., Claverie, J. M, Decelle, J., Dolan, J. R., Dunthorn, M., Edvardsen, B., Gobet, A., Kooistra, W. H., Mahé, F., Not, F., Ogata, H., Pawlowski, J., Pernice, M. C., Romac, S., Shalchian-Tabrizi, K., Simon, N., Stoeck, T., Santini, S., Siano, R., Wincker, P., Zingone, A., Richards, T. A., de Vargas, C. & Massana, R. 2014. Patterns of rare and abundant marine microbial eukaryotes. *Curr. Biol.* 24:813–21.Milne, I., Stephen, G., Bayer, M., Cock, P. J., Pritchard, L., Cardle, L., Shaw, P. D. & Marshall, D. 2013. Using Tablet for visual exploration of second-generation sequencing data. *Brief. Bioinform.* 14:193–202.

Mostaert, A. S., Karsten, U., Hara, Y. & Watanabe, M. M. 1998. Pigments and fatty acids of marine raphidophytes: A chemotaxonomic re-evaluation. *Phycol. Res.* 46:213–20.

Muñoz-Gómez, S. A., Mejía-Franco, F. G., Durnin, K., Colp, M., Grisdale, C. J., Archibald, J. M. & Slamovits, C. H. 2017. The new red algal subphylum Proteorhodophytina comprises the largest and most divergent plastid genomes known. *Curr. Biol*. 27:1677–84.e4.

Nguyen, L.T., Schmidt, H. A., von Haeseler, A. & Minh, B. Q. 2015. IQ-TREE: a fast and effective stochastic algorithm for estimating maximum-likelihood phylogenies. *Mol. Biol. Evol*. 32:268–74.

Noguchi, F., Tanifuji, G., Brown, M. W., Fujikura, K. & Takishita, K. 2016. Complex evolution of two types of cardiolipin synthase in the eukaryotic lineage stramenopiles. *Mol. Phylogenet. Evol*. 101:133–41.

Obiol, A., Giner, C. R., Sánchez, P., Duarte, C. M., Acinas, S. G. & Massana, R. 2020. A metagenomic assessment of microbial eukaryotic diversity in the global ocean. *Mol. Ecol. Resour.* 20:718–31.

Ohta, N., Matsuzaki, M., Misumi, O., Miyagishima, S., Nozaki, H., Tanaka, K., Shin-I, T., Kohara, Y., Kuroiwa, T. 2003. Complete sequence and analysis of the plastid genome of the unicellular red alga *Cyanidioschyzon merolae*. *DNA Res*. 10:137.

Okumura, Y., Yamasaki, M. & Suzuki, T. 2001. Pigment profile and violaxanthin cycle of *Heterosigma akashiwo* (Raphidophyceae). *J. Shellfish Res.* 20:1263–68.

Přibyl, P., Eliáš, M., Cepák, V., Lukavský, J. & Kaštánek, P. 2012. Zoosporogenesis, morphology, ultrastructure, pigment composition, and phylogenetic position of *Trachydiscus minutus* (Eustigmatophyceae, Heterokontophyta). *J. Phycol.* 48:231–42.

Rambaut, A. 2009. FigTree v1.4.2: Tree Figure Drawing Tool. Available: http://tree.bio.ed.ac.uk/software/figtree.

Reumann, S., Inoue, K. & Keegstra, K. 2005. Evolution of the general protein import pathway of plastids (review). *Mol. Membr. Biol*. 22:73–86.

Reynolds, E. S. 1963. The use of lead citrate at high pH as an electron-opaque stain in electron microscopy. *J. Cell Biol.* 17:208–12.

Rodríguez, F., Chauton, M., Johnsen, G., Andresen, K., Olsen, L. M. & Zapata, M. 2006. Photoacclimation in phytoplankton: implications for biomass estimates, pigment functionality and chemotaxonomy. *Mar. Biol.* 148:963–71.

Ronquist, F. & Huelsenbeck, J. P. 2003. MrBayes 3: Bayesian phylogenetic inference under mixed models. *Bioinformatics* 19:1572–4.

Sasaki, Y., Sekiguchi, K., Nagano, Y. & Matsuno, R. 1993. Chloroplast envelope protein encoded by chloroplast genome. *FEBS Lett*. 316:93–8.

Schultz, J., Maisel, S., Gerlach, D., Müller, T. & Wolf M. 2005. A common core of secondary structure of the internal transcribed spacer 2 (ITS2) throughout the Eukaryota. *RNA* 11:361–4.

Seibel, P. N., Müller, T., Dandekar, T. & Wolf, M. 2008. Synchronous visual analysis and editing of RNA sequence and secondary structure alignments using 4SALE. *BMC Res. Notes* 1:91.

Seoane, S., Zapata, M. & Orive, E. 2009. Growth rates and pigment patterns of haptophytes isolated from estuarine waters. *J. Sea Res.* 62:286–94.

Sibbald, S. J. & Archibald, J. M. 2020. Genomic insights into plastid evolution. *Genome Biol. Evol.* 12:978–90.

Stoeck, T. & Epstein, S. 2003. Novel eukaryotic lineages inferred from small-subunit rRNA analyses of oxygen-depleted marine environments. *Appl. Environ. Microbiol*. 69:2657–63.

Ševčíková, T., Horák, A., Klimeš, V., Zbránková, V., Demir-Hilton, E., Sudek, S., Jenkins, J., Schmutz, J., Přibyl, P., Fousek, J., Vlček, Č., Lang, B. F., Oborník, M., Worden, A.Z. & Eliáš, M. 2015. Updating algal evolutionary relationships through plastid genome sequencing: did alveolate plastids emerge through endosymbiosis of an ochrophyte? *Sci. Rep*. 5:10134.

Ševčíková, T., Yurchenko, T., Fawley, K. P., Amaral, R., Strnad, H., Santos, L. M. A., Fawley M. W. & Eliáš, M. 2019. Plastid genomes and proteins illuminate the evolution of eustigmatophyte algae and their bacterial endosymbionts. *Genome Biol. Evol.* 11:362–79.

Tajima, N., Saitoh, K., Sato, S., Maruyama, F., Ichinomiya, M., Yoshikawa, S., Kurokawa, K., Ohta, H., Tabata, S., Kuwata, A. & Sato, N. 2016. Sequencing and analysis of the complete organellar genomes of Parmales, a closely related group to Bacillariophyta (diatoms). *Curr. Genet*. 62:887–96.

Takishita, K., Yamaguchi, H., Maruyama, T. & Inagaki, Y. 2009. A hypothesis for the evolution of nuclear-encoded, plastid-targeted glyceraldehyde-3-phosphate dehydrogenase genes in "chromalveolate" members. *PLoS ONE* 4:e4737.

Taylor F. J. R. 1992. The taxonomy of harmful marine phytoplankton. *Giorn. Bot. Ital.* 126:209–19.

Tong, S. M. 1995. *Developayella elegans* nov. gen., nov. spec., a new type of heterotrophic flagellate from marine plankton. *Eur. J. Protistol.* 31:24–31.

Tyrrell, J. V. 1999. Molecular probes for the fish-killing raphidophytes and the phylogeny of the group. Master's thesis. The University of Auckland, Auckland.

Tyrrell, J. V., Bergquist, P. R., Bergquist, P. R. & Scholin, C. A. 2001. Detection and enumeration of *Heterosigma akashiwo* and *Fibrocapsa japonica* (Raphidophyceae) using rRNA-targeted oligonucleotide probes. *Phycologia* 40:457-67.

Vesk, M. & Moestrup, O. 1987. The flagellar root system in *Heterosigma akashiwo* (Raphidophyceae). *Protoplasma* 137:15–28.

Wang, H. C., Minh, B. Q., Susko, E. & Roger, A. J. 2018. Modeling site heterogeneity with posterior mean site frequency profiles accelerates accurate phylogenomic estimation. *Syst. Biol.* 67:216–35.

Wetherbee, R., Jackson, C. J., Repetti, S. I., Clementson, L. A., Costa, J. F., van de Meene, A., Crawford, S. & Verbruggen, H. 2019. The golden paradox – a new heterokont lineage with chloroplasts surrounded by two membranes. *J. Phycol.* 55:257–78.

Wild, P., Schraner, E. M., Adler, H. & Humbel, B. M. 2001. Enhanced resolution of membranes in cultured cells by cryoimmobilization and freeze-substitution. *Microsc. Res. Tech.* 53:313–21.

Wu, W., Wang, L., Liao, Y. & Huang, B. 2015. Microbial eukaryotic diversity and distribution in a river plume and cyclonic eddy-influenced ecosystem in the South China Sea. *MicrobiologyOpen* 4:826–40.

Yamaguchi, H., Hoppenrath, M., Takishita, K. & Horiguchi, T. 2008. *Haramonas pauciplastida* sp. nov. (Raphidophyceae, Heterokontophyta) and phylogenetic analyses of *Haramonas* species using small subunit ribosomal RNA gene sequences. *Phycol. Res.* 56:127–38.

Yamaguchi, H., Nakayama T., Murakami, A. & Inouye, I. 2010. Phylogeny and taxonomy of the Raphidophyceae (Heterokontophyta) and *Chlorinimonas sublosa* gen. et sp. nov., a new marine sand-dwelling raphidophyte. *J. Plant Res.* 123:333–42.

Yang, E. C., Boo, G. H., Kim, H. J., Cho, S. M., Boo, S. M., Andersen, R. A. & Yoon, H. S. 2012. Supermatrix data highlight the phylogenetic relationships of photosynthetic stramenopiles. *Protist* 163:217–31.

Zapata, M., Rodríguez, F. & Garrido, J. L. 2010. Separation of chlorophylls and carotenoids from marine phytoplankton: a new HPLC method using a reversed phase C_8 column and pyridine-containing mobile phases. *Mar. Ecol. Prog. Ser.* 195:29–45.

Zimmermann, L., Stephens, A., Nam, S. Z., Rau, D., Kübler, J., Lozajic M., Gabler F., Söding, J., Lupas A. N. & Alva V. 2018. A completely reimplemented MPI bioinformatics toolkit with a new HHpred server at its core. *J. Mol. Biol*. 430: 2237–43.

Table 1. Previously published or released sequences attributed to *Olisthodiscus luteus*. The genotype K-0444 corresponds to bona fide *O. luteus*, the genotype NIES-15 is here described as a new species, *O. tomasii*.

Accession number	Gene	Strain	Reference	Genotype	Notes
M24288.1	*rbc*S, *rbc*L	-	Boczar et al. 1989	-	*Heterosigma akashiwo*
X15768.1	16S rRNA, 23S rRNA	pOCX8.1	Delaney and Cattolico 1989	-	*Heterosigma akashiwo*
M82860.1	16S rRNA	-	Delaney and Cattolico 1991	-	*Heterosigma akashiwo*
AF086950.1	28S rRNA	NIES-15	submitted by L. Connell, 1998 (no associated publication found)	NIES-15	differs by one single-nucleotide deletion from the reference sequence, perhaps a sequencing error
AF157380.1	18S-ITS1-5.8S rRNA-ITS2	K-0444	Connell 2000	K-0444	two mismatches from the reference sequence at the 5' end, probably sequencing errors
AF210743.1	28S rRNA	NIES-15	Tyrrell et al. 2001	NIES-15	five single-nucleotide indels at the sequence termini compared to the

					reference sequence, perhaps sequencing errors
AF112992.1	18S-ITS1-5.8S rRNA-ITS3	NIES-15	Connell 2002	NIES-15	differs from the reference sequence by multiple insertions and two mismatches (sequencing errors or intragenomic heterogeneity)
AY788937.1	18S rRNA	NIES-15	Bowers et al. 2006	K-0444	differs by one single-nucleotide deletion, perhaps a sequencing error
DQ065612.1	ITS1-5.8S rRNA-ITS2	NIES-15	Bowers et al. 2006 (the sequence not mentioned in the paper)	K-0444	differs by one ambiguous position (Y at place of T in the reference sequence)
AY864022.1	16S rRNA	C. Tomas Japan	Bowers et al. 2006 (the sequence not mentioned in the paper)	K-0444	100% identity with K-0444 (no NIES-15 sequence for comparison)
AB280605.1	*rbc*L	NIES-15	Iida et al. 2007	NIES-15	57 mismatches compared to the K-0444 sequence
AB459521.1	GapC1	NIES-15	Takishita et al. 2009	NIES-15	96 mismatches in the coding sequence compared to K-0444

AB459522.1	GapC2	NIES-15	Takishita et al. 2009	NIES-15	163 mismatches in the coding sequence compared to K-0444

Figure 1. Light microscopy of *Olisthodiscus* spp.: (A-L) *Olisthodiscus luteus* strain K-0444 and (M-X) *O. tomasii* sp. nov., strain NIES-15. (A-B) Roundish vegetative cells containing a central nucleus and showing an orange extraplastidial globule (A) and pyrenoids (B). (C-D) Broadly ellipsoidal vegetative cell with an extraplastidial orange globule (C) and small protrusions (D). (E) Two unequal flagella emerging sub-anteriorly. (F) Pyriform cell with a prominent nucleus. (G) Ready-to-divide cell containing two sets of flagella and nuclei. (H) Two cells almost separated by the longitudinal fission. (I) Cell with a "pseudopodium" containing a plastid. (J) Cell with shrunken plastids. (K) Honeycomb-like arrangement of cytoplasmic vesicles. (L) Zoosporangium with prominent septa. (M) Roundish vegetative cell with a prominent red extraplastidial globule and pyrenoids. (N) Ellipsoidal cell. (O) Ovoid cell with a huge extraplastidial globule and a central nucleus. (P) Bead-like protrusions. (Q) Ready-to-divide cells with duplicated flagella and nuclei. (R) Cells almost separated by fission. (S) Cell with cytoplasmic vesicles and small protrusions. (T) Putative cyst with crenate protuberances. (U) Cell dividing after a dormant period. (V-W) Zoospores containing two (V) or a single plastid (W). (X) Dead cell with remnant ring of plastids. Abbreviations: eg – extraplastidial globule, N – nucleus, nu – nucleolus, py – pyrenoid, af – anterior flagellum, p – posterior flagellum, pr – protrusion, ps – "pseudopodium", cv – cytoplasmic vesicles, cpr – crenate protrusions. Scale bars = 5 μm.

Figure 2. Scanning electron micrographs of *Olisthodiscus* spp. (A–D). *Olisthodiscus luteus* strain K-0444. (A) Lateral view of cell showing convex dorsal and slightly concave ventral side with the funnel shaped depression where the heterokont flagella emerge. (B) Detail of anterior flagellum with hairs. Scattered scales are visible in the background (arrows). (C) Detail of cell surface covered in scales and fibrous structures. (D) Detail of flagella showing the swelling on the hairy flagellum. (E–G) *Olisthodiscus tomasii* strain NIES-15. (E) Cell with heterokont flagella. (F) Ventral view of cell with two flagella emerging from a funnel shaped depression. (G) Detail of cell surface showing scales and bead-like protrusions (arrowheads).

Figure 3. TEM images of *Olisthodiscus luteus* strain K-0444. (A) Longitudinal section of a cell showing general organization: plasmalemma covered by scales (arrowheads) and fibres (asterisks), peripheral vesicles (PV), microtubules (dashed arrows), membranous structures (MS), nucleus (N), parietal plastids (P) with pyrenoids (py) and Golgi apparatus (G). Cell protrusions (pr) covered by scales are notable. (B) System of peripheral vesicles (PV) interconnected by bridges

(arrows) and containing granular material. (C) Mastigonemes (MA) in ER vesicle and stack of membranes (MS) believed to develop into PVs. (D) Body scales consisting of seven subunits. (E) Body scales are pentagonal in cross section. (F) Fine ultrastructure of the Golgi apparatus and mature scales being packed in Golgi-derived vesicles (GDVs). (G) Cross section of the anterior flagellum with hairs. (H) Longitudinal section of the anterior flagellum with hairs in addition to scales and fibres reminiscent of that covering the cell body. Scale bars = 3 μm (A), 1 μm (B, C), 500 nm (F, G, H), 200 nm (D), 100 nm (E).

Figure 4. TEM images of *Olisthodiscus tomasii* strain NIES-15. (A, B) General ultrastructure of the cells, showing flagella (F), plastids (P) with pyrenoids (py), nucleus (N), Golgi apparatus (G) and mitochondria (m). (C) Fine ultrastructure of the Golgi apparatus showing GDVs where scales are packed for release. (D) Zoospore containing two plastids and covered by multiple layers of scales (arrowheads). (E) Scales connected by a mesh of fibrils (asterisks), and a peripheral vesicle (PV) containing electron-dense granules. (F) Cytoplasmic vesicles (cv) occupying most of the cell volume and containing an amorphous material. (G) Scales composed of six subunits (arrowhead). Plastid surrounded by four membranes and membranous structures (MS) sandwiched between the plastid and plasmalemma. (H) Anterior (AB) and posterior (PB) basal bodies overlapping in counter-clockwise orientation and transverse section of the flagellar root 1 (R1) associated with the anterior flagellum. Double scale is marked (white arrowhead). (I) Cross section of the anterior flagellum with hairs. Scale bars = 2 μm (A, B, F), 1 μm (C, D), 500 nm (E, H), 200 nm (G, I).

Figure 5. Bayesian phylogenetic tree based on a concatenated dataset of 18S and partial 28S rRNA gene sequences showing all ochrophyte algae classes. Support values are shown near the nodes as follows: Bayesian posterior probability/ML bootstrap.

Figure 6. Phylogenetic position of *Olisthodiscus luteus* as indicated by plastid genome-encoded markers. (A) Phylogeny of ochrophytes inferred from a concatenated alignment of 69 plastid genome-encoded conserved proteins. The tree topology shown was inferred by using PhyloBayes (CAT+GTR model). Branch support values (posterior probabilities calculated by PhyloBayes and non-parametric bootstrap values obtained with IQ-TREE) are shown only for branches where any of the values was not maximal (i.e., 1/100). The tree is rooted with an outgroup (not shown) represented by selected species of haptophytes, cryptophytes, and red algae. (B) Phylogeny of

ochrophytes inferred from a concatenated alignment of products of seven conserved plastid genes, including amino acid sequences of five proteins (*Rbc*L, *Psa*A, *Psb*A, *Psb*C, *Cbb*X) and nucleotide sequences of 16S and 23S rRNA. The tree was obtained by using IQ-TREE, with each gene representing a separate partition (for the selection of the optimal substitution model and estimation of the free parameters). Non-parametric bootstrap values are shown at branches when ≥50%. The tree is rooted with an outgroup (not shown) represented by selected species of haptophytes, cryptophytes, red algae and glaucophytes.

Figure 7. Map of the plastid genome of *Olisthodiscus luteus* K-0444. Genes are shown as boxes (colored according to the functional category they belong to; see the graphical legend in the bottom left corner) facing inward or outward of the circle depending on whether they are transcribed in the clockwise or counter-clockwise direction, respectively. The internal circle in grey indicates the variation in the GC content along the plastid genome. The surprisingly present *cysT-cysW* gene pair is highlighted with a red arrow. IRA and IRB: inverted repeats; LSC and SSC: large and small single-copy regions, respectively.

Figure 8. Pigment composition of *Olisthodiscus* strains. (A) Chromatogram (absorbance 440 nm) showing the pigment composition of *O. luteus,* strain K-0444. (B) Chromatogram (absorbance 440 nm) showing the pigment composition of *O. luteus,* strain NIES-15. Chl: chlorophyll; Viola: violaxanthin; Fuco: fucoxanthin; Anthera: antheraxanthin; Zea: zeaxanthin; Car: carotene.

Figure S1. ITS2 rDNA secondary structure of *Olisthodiscus tomasii* NIES-15. Positions that were variable between NIES-15 and *O. luteus* K-0444 are shown as empty circles, insertions found in K-0444 are indicated by an arrowhead, together with their length in bp. Deletions found in K-0444 are indicated by X. Four CBCs are marked by two opposing filled circles.

Figure S2. Metabarcodes (V9 regions of the 18S rRNA gene) from organisms potentially related to *Olisthodiscus*. The most likely position of these short (131 or 132 bp) sequences (highlighted in bold) on a reference 18S rRNA tree of ochrophytes (for the original tree with branch support values see Fig. S5) was determined by the EPA algorithm implemented in RAxML. The origin and nucleotide sequences of the metabarcodes are available in Table S5.

Figure S3. Phylogenetic analysis of CysT and CysW proteins. The tree was inferred with the ML method implemented in IQ-TREE (with the LG+F+G4 substitution model). Bootstrap values are displayed if ≥50%, the root is placed arbitrarily. Sequences from eukaryotes are rendered in colour according to the taxon, *Olisthodiscus luteus* K-0444 – orange with a grey background, green algae and plants – green, red algae – red.

Figure S4. Conserved genomic position of *cysT* and *cysW* genes in plastid genomes of *Olisthodiscus luteus* and cyanidiophytes. The *crtR* gene is absent from the *O. luteus* plastid genome due to loss, making *cysW* and *ycf54* immediate neighbours. Note that the *ctrR* gene (encoding β-carotene hydroxylase) is annotated with an alternative name *desA* in the *G. sulphuraria* plastid genome. GenBank accession numbers of the plastid genomes analysed: *C. merolae* - NC_004799.1; Cyanidiaceae sp. MX-AZ01 - KJ569775.1; *G. sulphuraria* - NC_024665.1.

Figure S5. Maximum likelihood phylogenetic tree based on 18S rRNA gene sequences showing all ochrophyte algae classes, including all sequenced species of the class Raphidophyceae. Sequences which were not used in the Figure 5 are indicated with accession numbers. Table S3 provides accession numbers of the rest of the sequences. Support values are shown near the nodes as follows: ML bootstrap (>50)/Bayesian posterior probability (≥0.9).

Figure S6. Phylogenetic analysis of Cem, proteins. The tree was inferred with the ML method implemented in IQ-TREE (with the JTT+F+I+G4 substitution model). Bootstrap values are displayed if ≥50%, the root is placed arbitrarily. Sequences are rendered in colour according to the taxon: ochrophytes – orange (*Olisthodiscus luteus* K-0444 highlighted with a grey background), green algae and plants – green, red algae – red, cryptophytes – brown, Cyanobacteria – blue.

Figure S7. Phylogenetic analysis of CysA proteins. The tree was inferred with the ML method implemented in IQ-TREE (with the LG+I+G4 substitution model). Bootstrap values are displayed if ≥50%, the root is placed arbitrarily. Sequences are rendered in colour according to the taxon: *Olisthodiscus luteus* K-0444 – orange (highlighted with a grey background), green algae and plants – green, red algae – red, Cyanobacteria – blue, other bacteria – black.

Figure S8. Phylogenetic analysis of Sbp proteins. The tree was inferred with the ML method implemented in IQ-TREE (with the LG+I+G4 substitution model). Bootstrap values are displayed if ≥50%, the root is placed arbitrarily. Sequences are rendered in colour according to the taxon: *Olisthodiscus luteus* K-0444 – orange (highlighted with a grey background), green algae and plants – green, red algae – red, Cyanobacteria – blue, other bacteria – black.

Table S1. Primers used for NIES-15 rDNA amplification and sequencing.

Table S2. Genes identified in plastid genomes of *Olisthodiscus luteus* and selected other ochrophytes.

Table S3. Accession numbers of 18S and 28S rRNA genes used for phylogenetic analysis.

Table S4. Accession numbers of plastid gene sequences used in phylogenetic analysis from species not represented by complete plastid genome sequences.

Table S5. V9 rDNA barcodes from organisms with putative specific relationship to *Olisthodiscus*.

Table S6. The *ycf80* gene in plastid genomes.

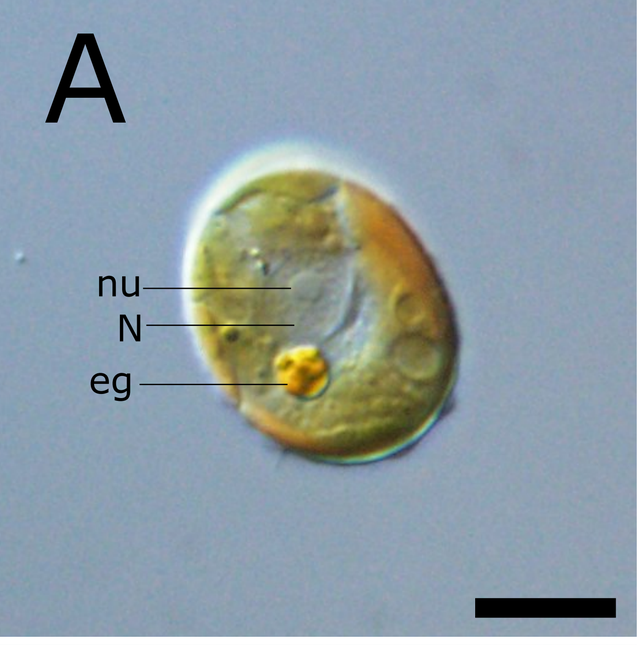
A
nu
N
eg

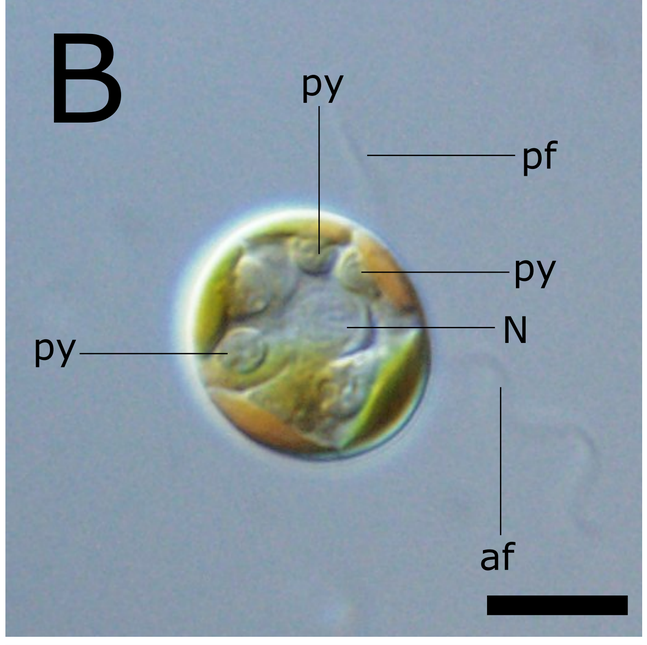
B
py
pf
py
py
N
af

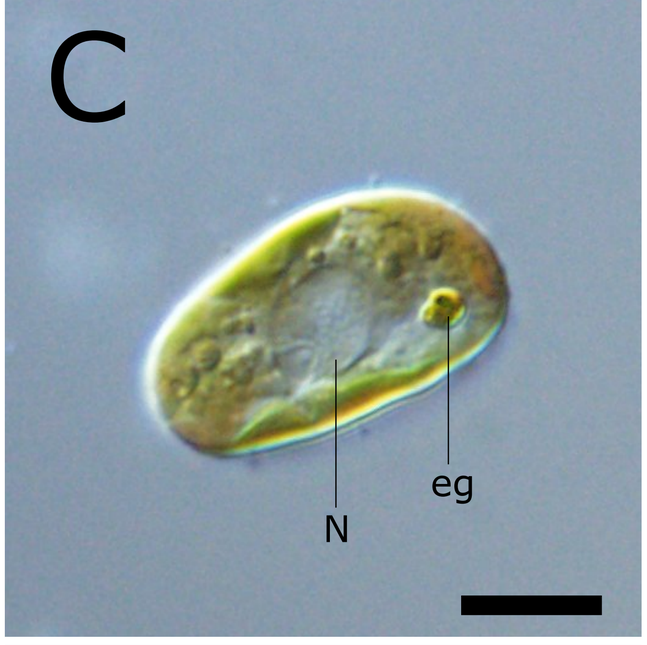
C
N
eg

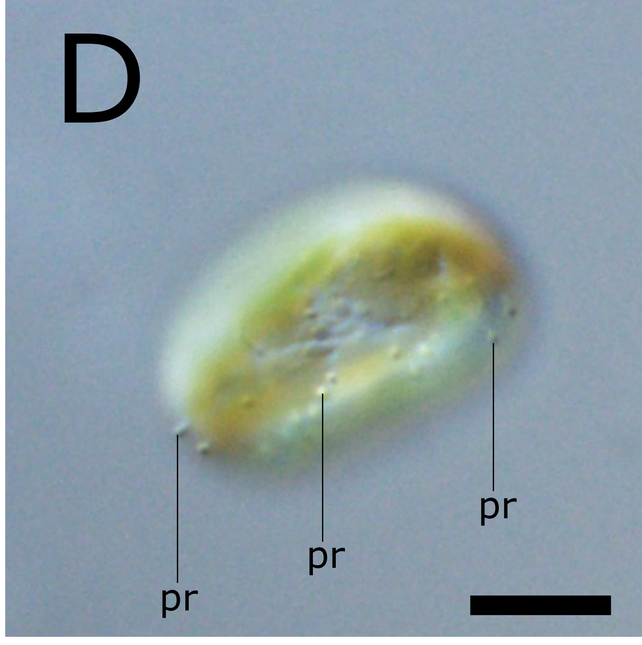
D
pr
pr
pr

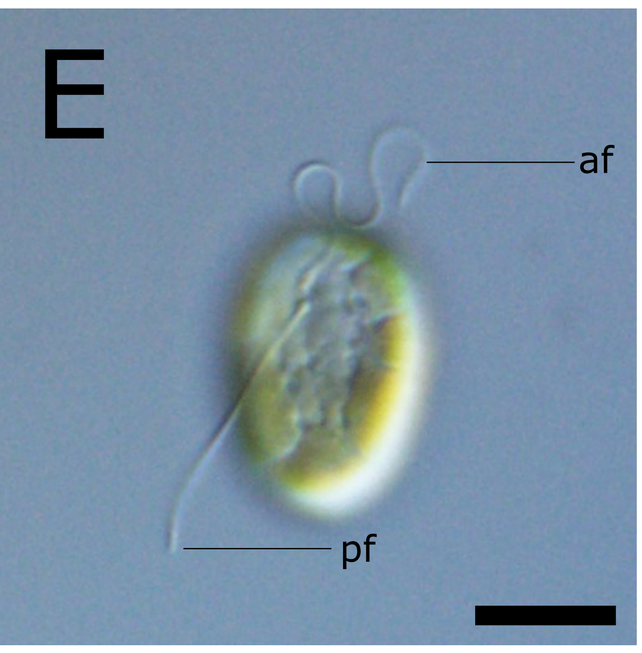
E
af
pf


F
N


G
af
af
pf
N
pf
N

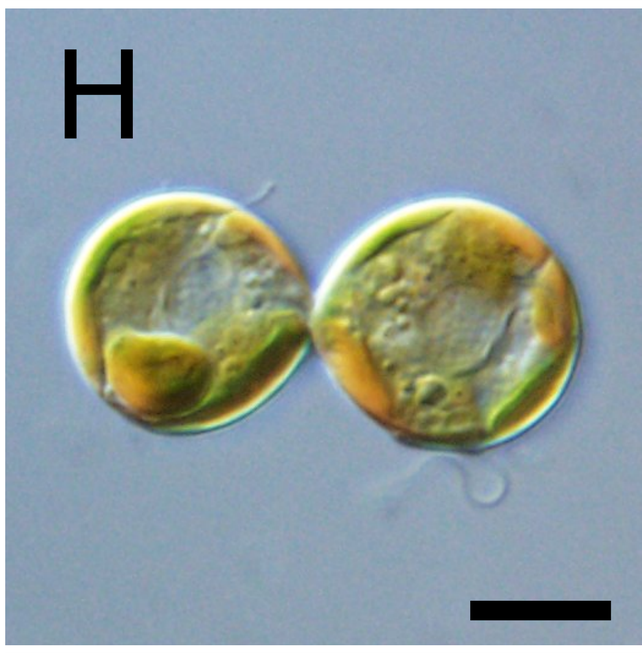
H

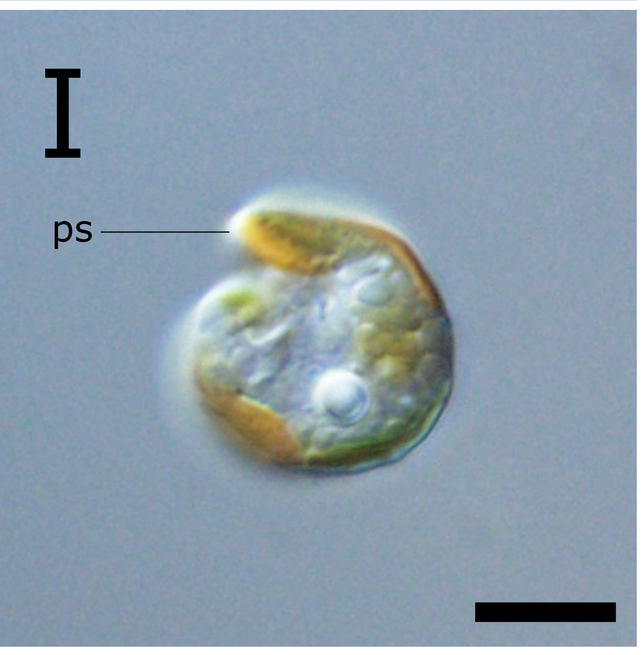
I
ps

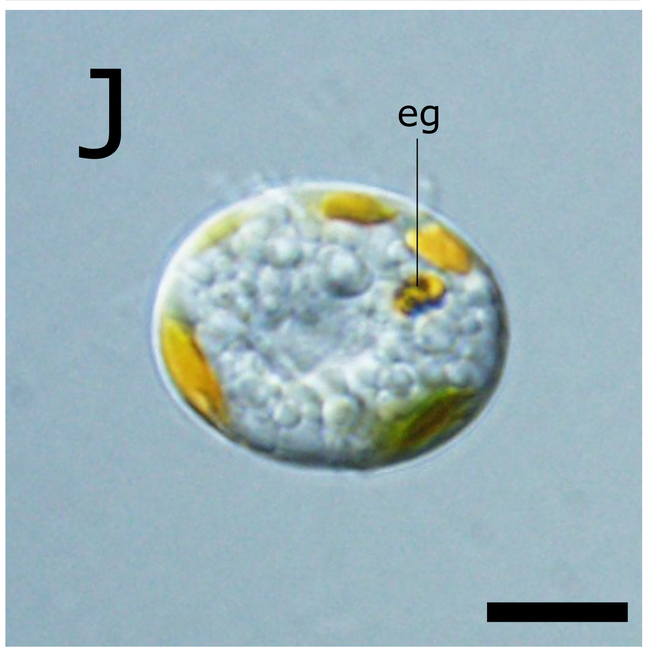
J
eg

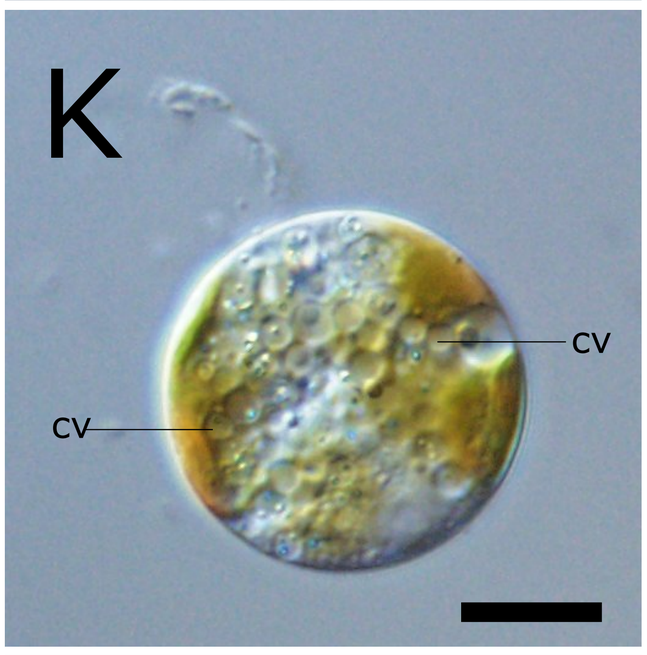
K
cv
cv

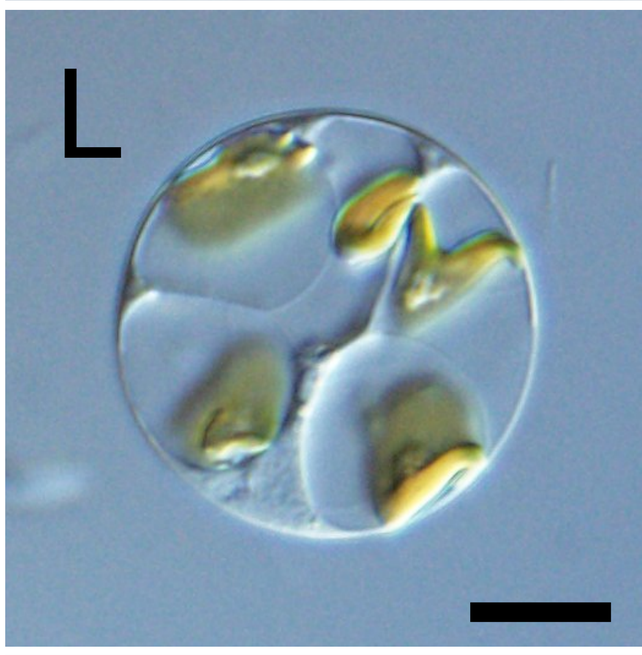
L

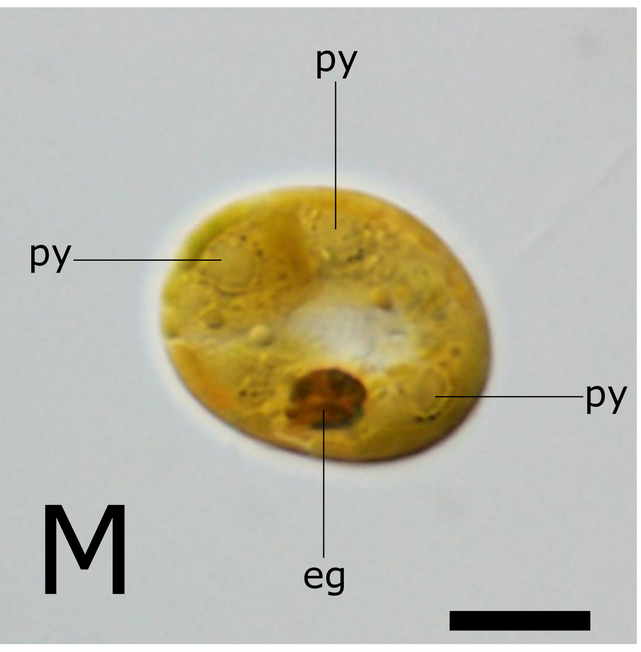
M
py
py
py
eg


N


O
N
eg

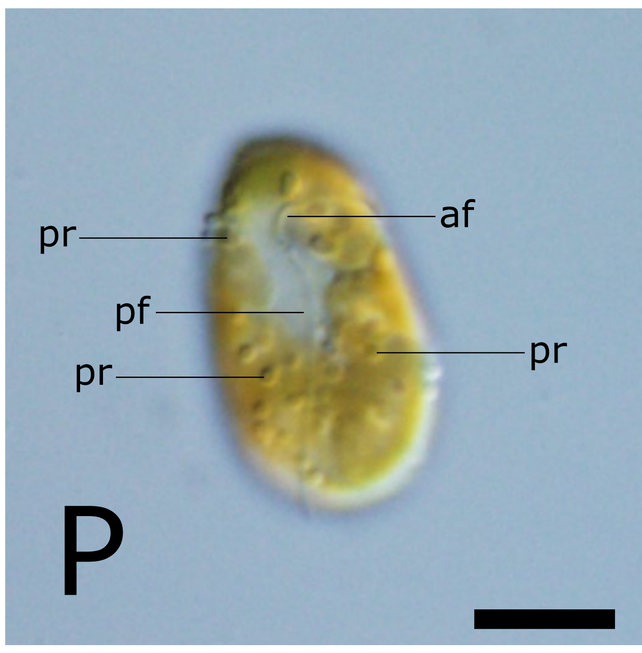
P
af
pr
pf
pr
pr

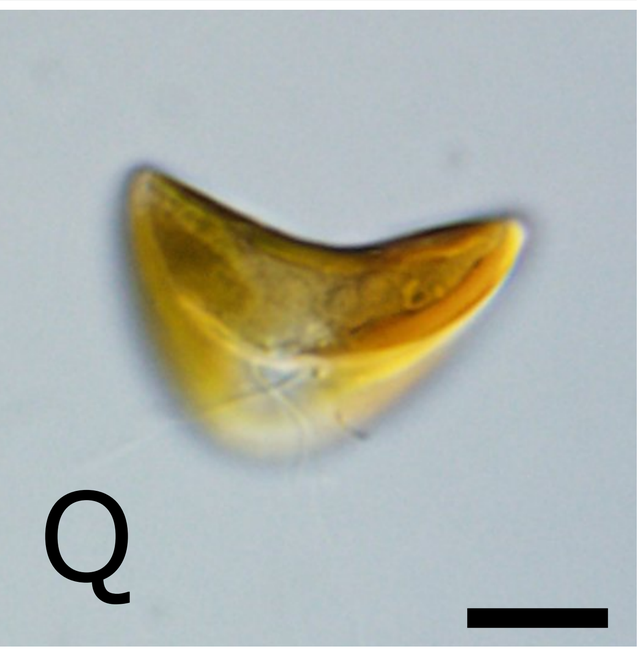
Q

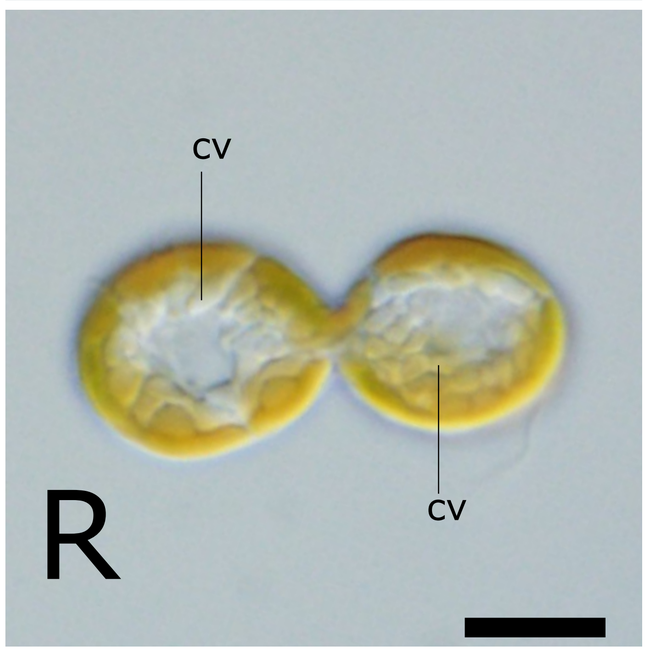
R
cv
cv

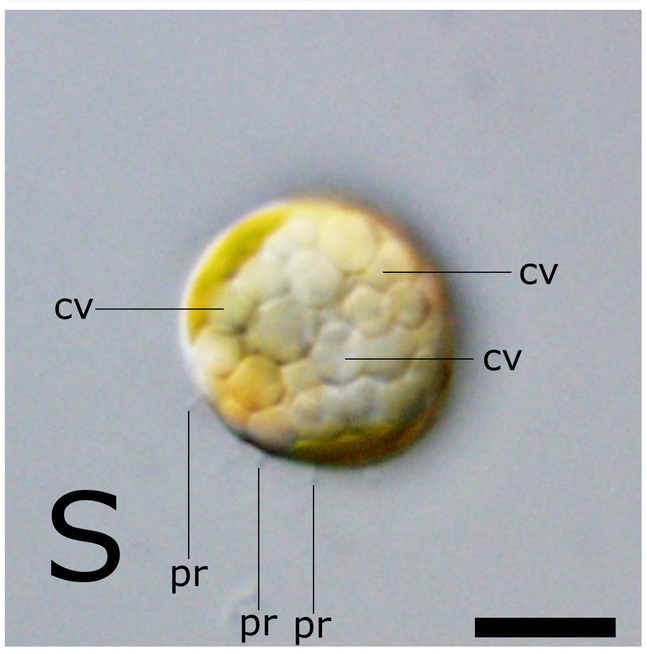
S
cv
cv
cv
pr
pr
pr

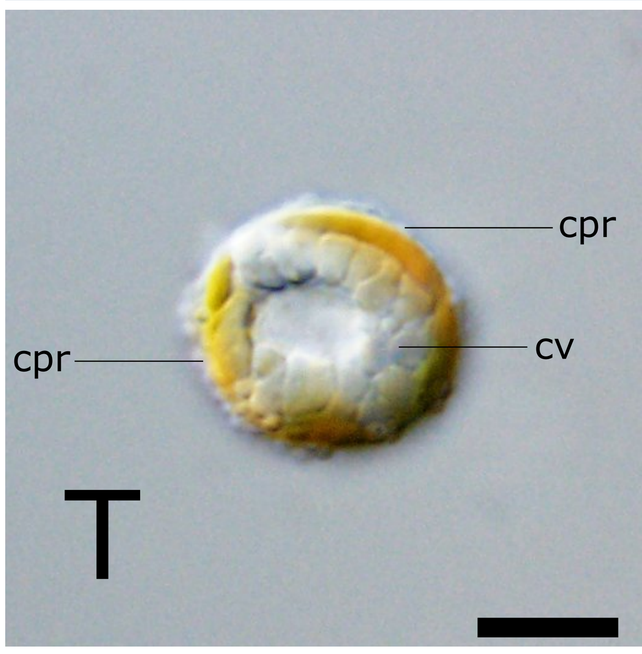
T
cpr
cpr
cv

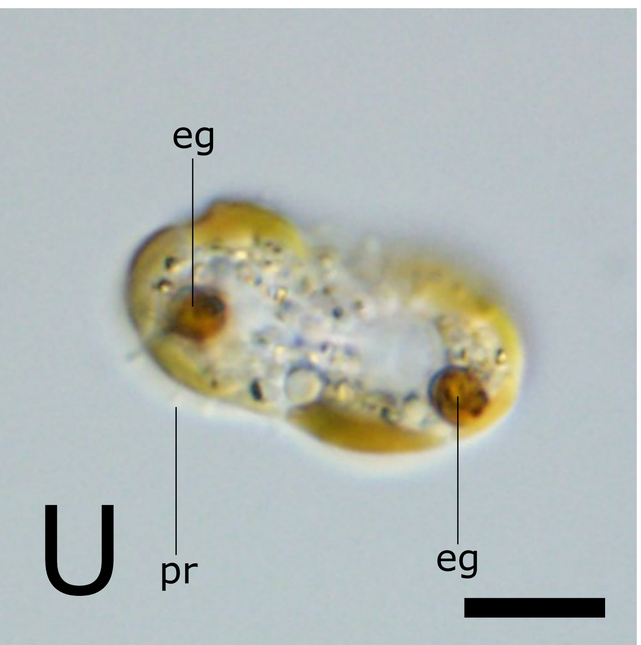
U
eg
pr
eg

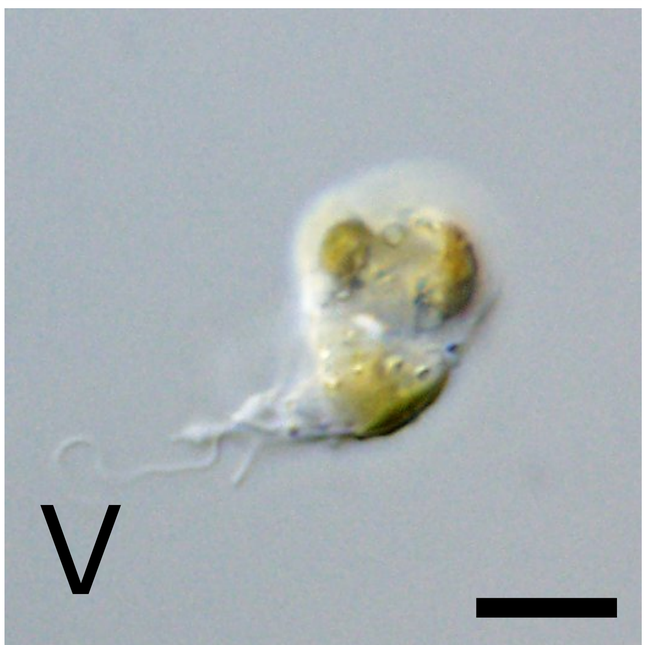
V

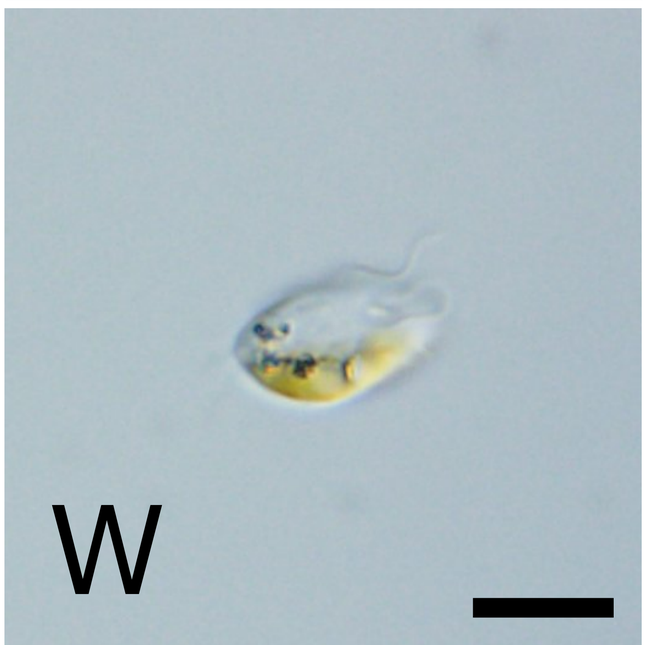
W

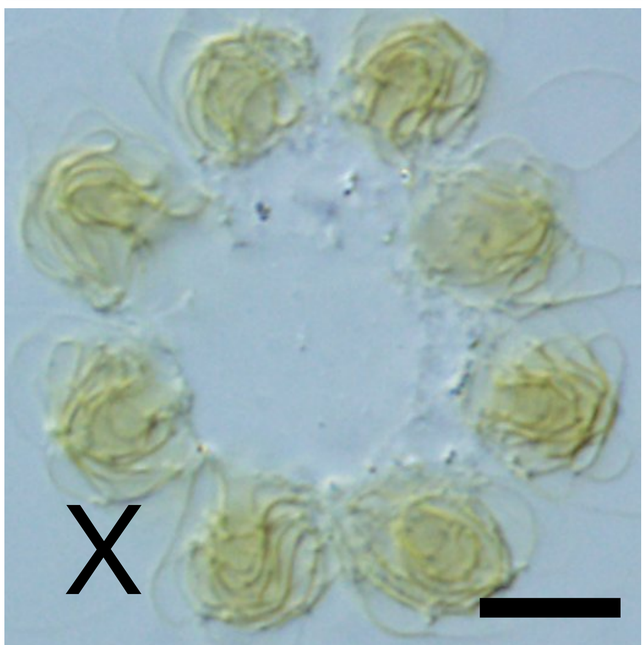
X

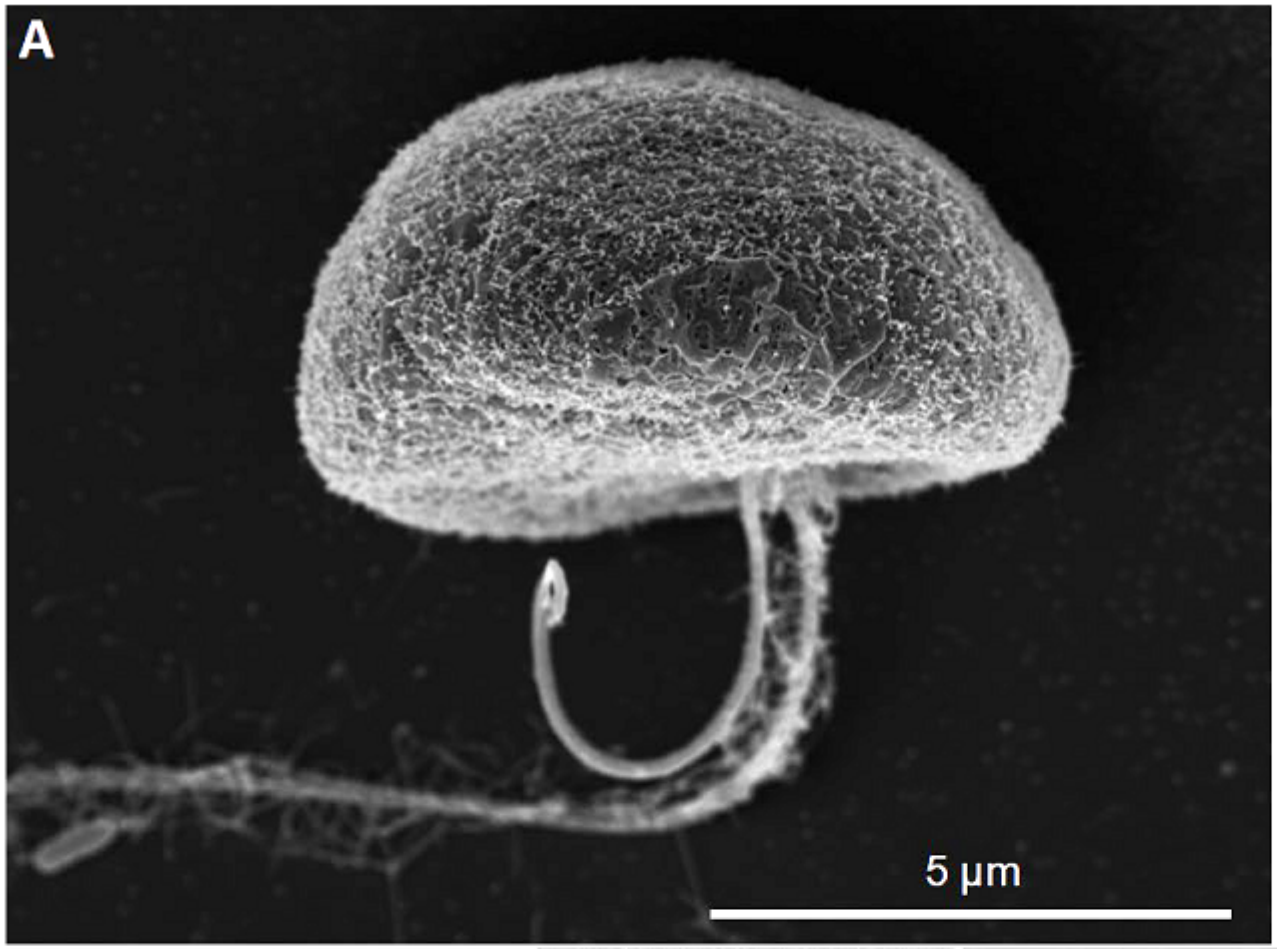
A
5 µm

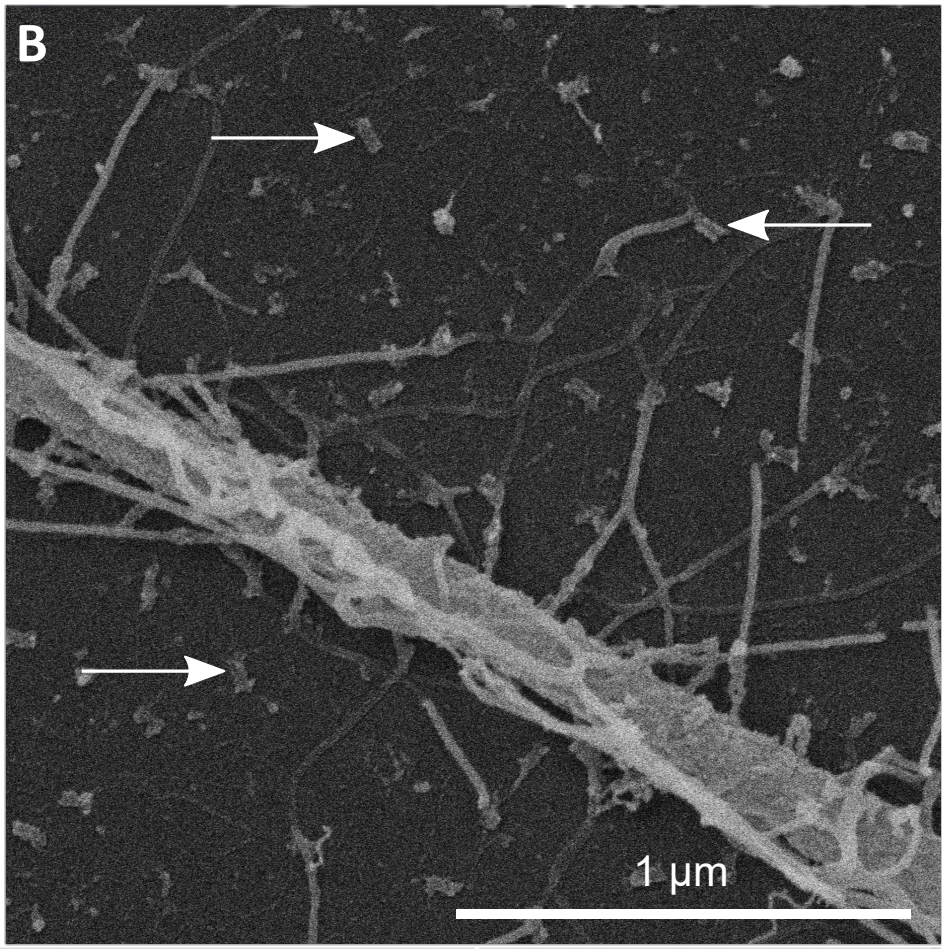
B
1 µm

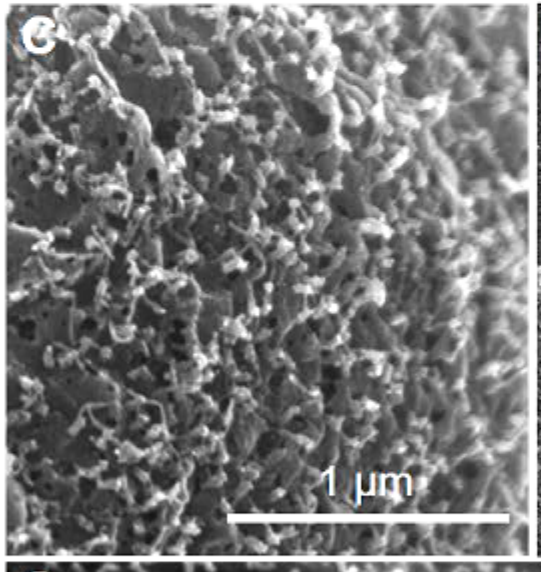
C
1 µm

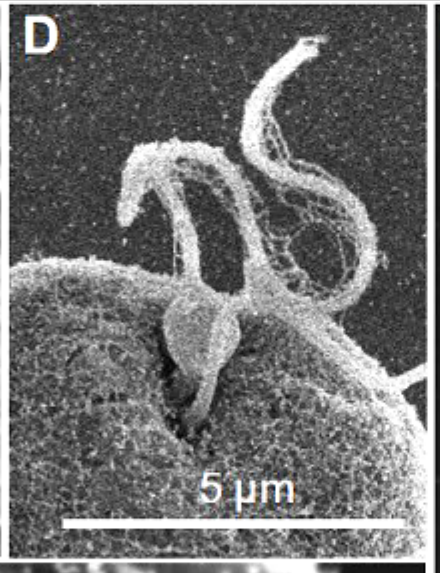
D
5 µm

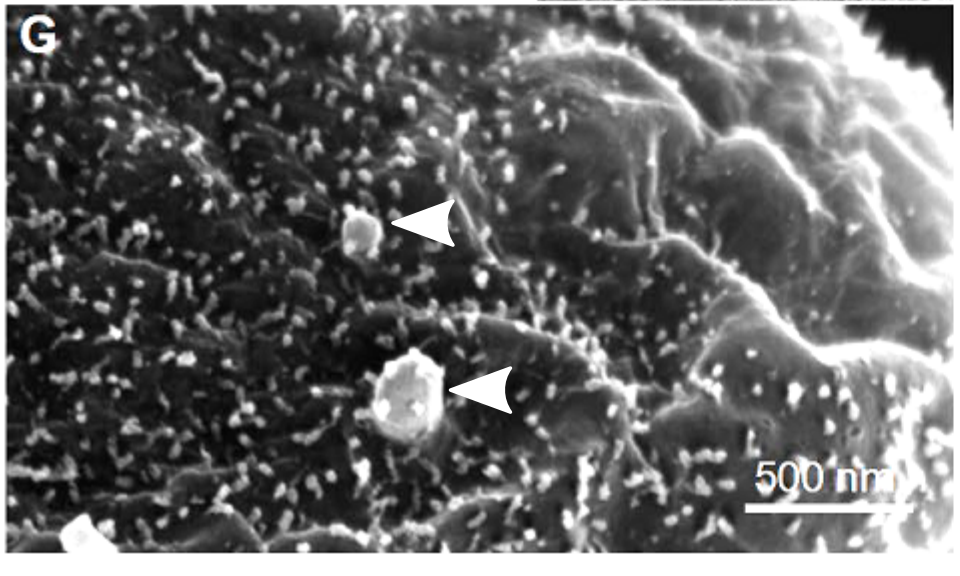
G
500 nm

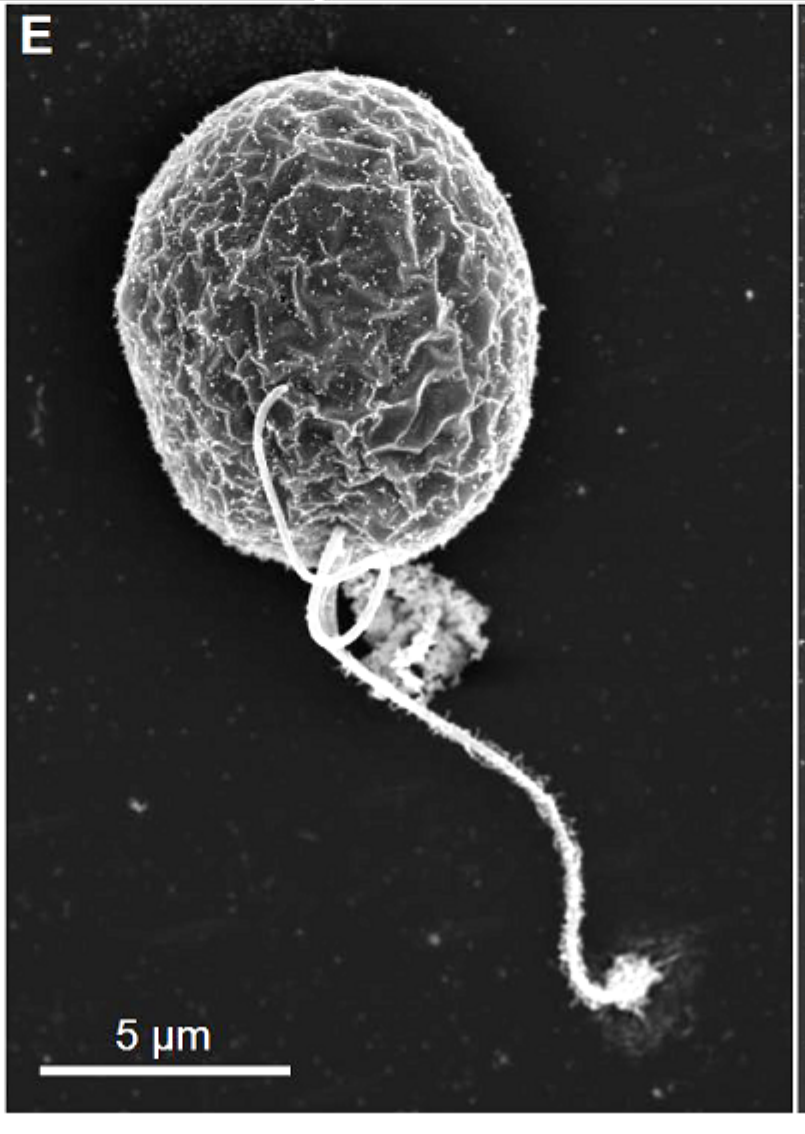
E
5 µm

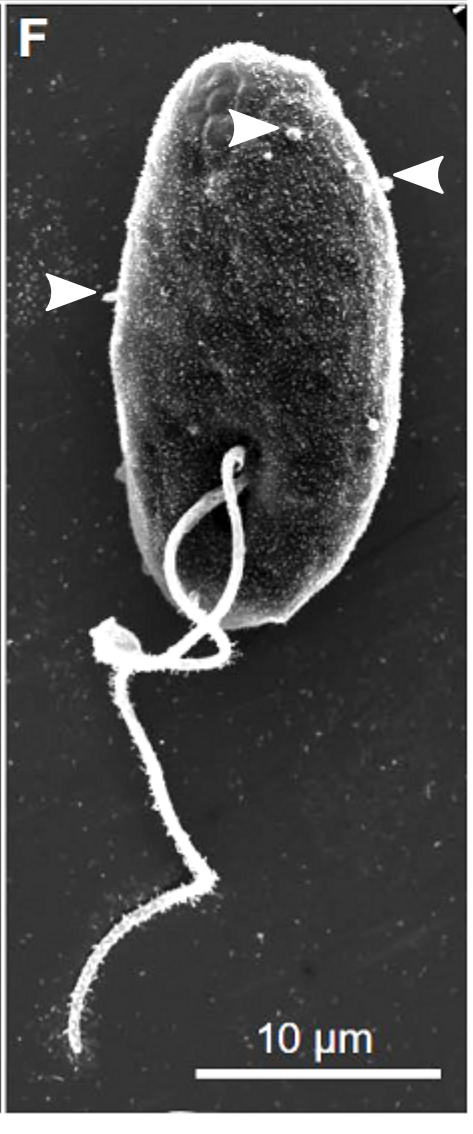
F
10 µm

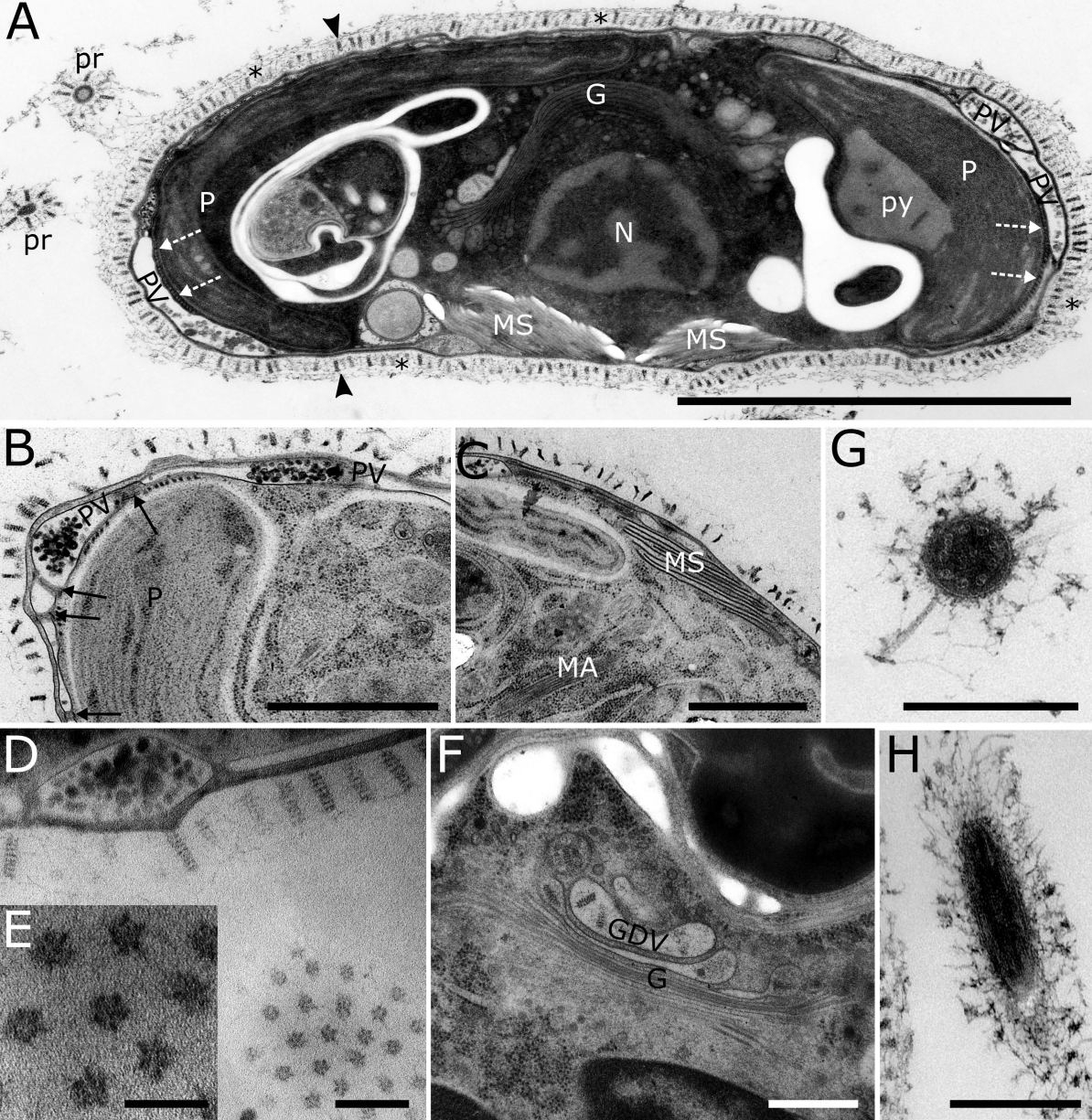
A
pr
pr
G
P
P
N
py
PV
PV
PV
MS
MS
B
PV
PV
P
C
MS
MA
G
D
E
F
GDV
G
H

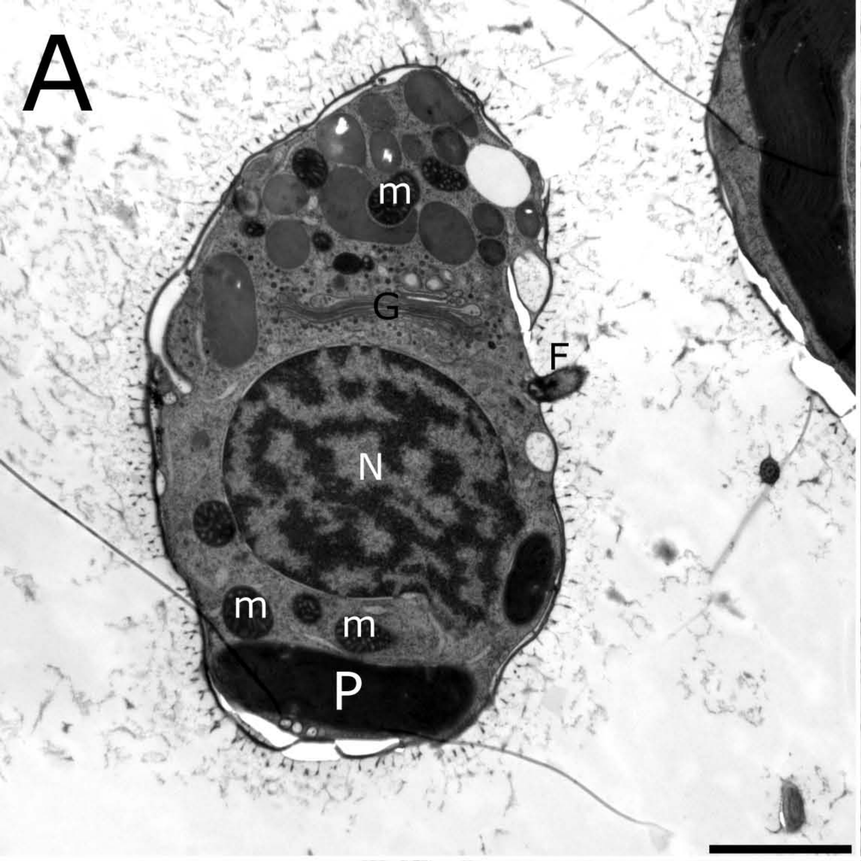
A
m
G
F
N
m
m
P

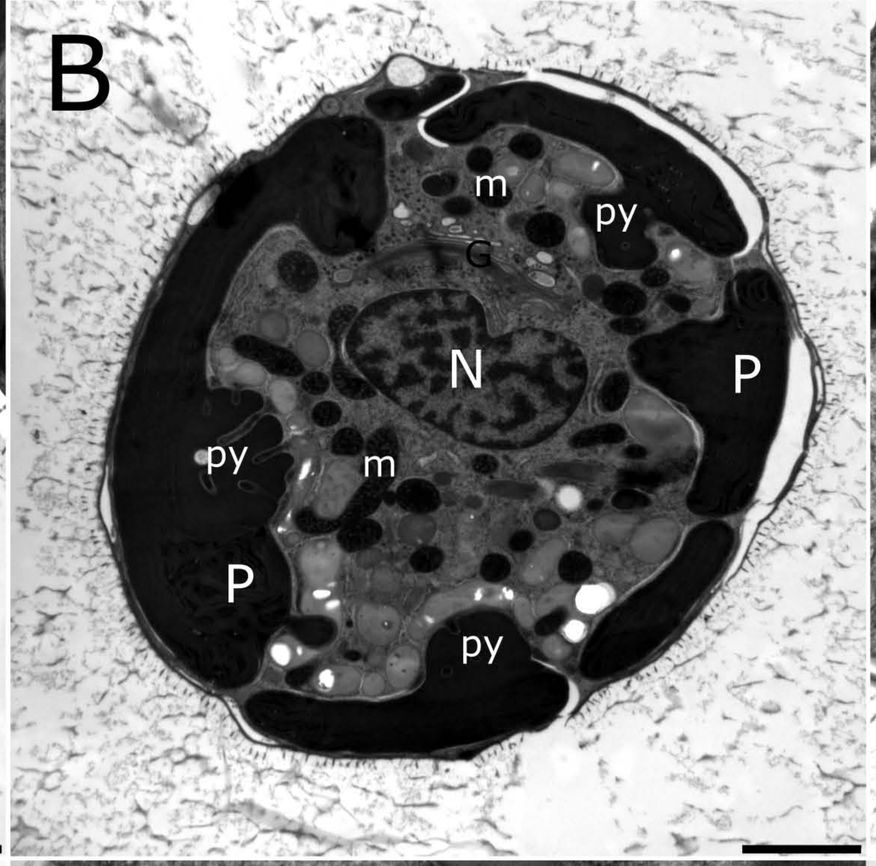
B
m
py
G
N
P
py
m
P
py

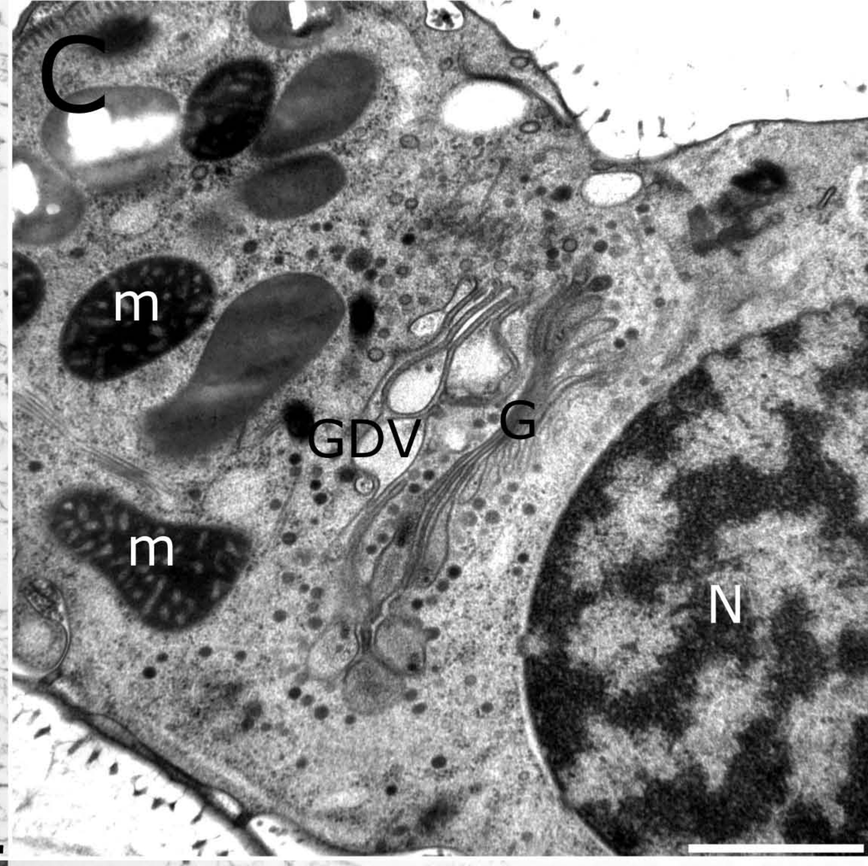
C
m
GDV
G
m
N

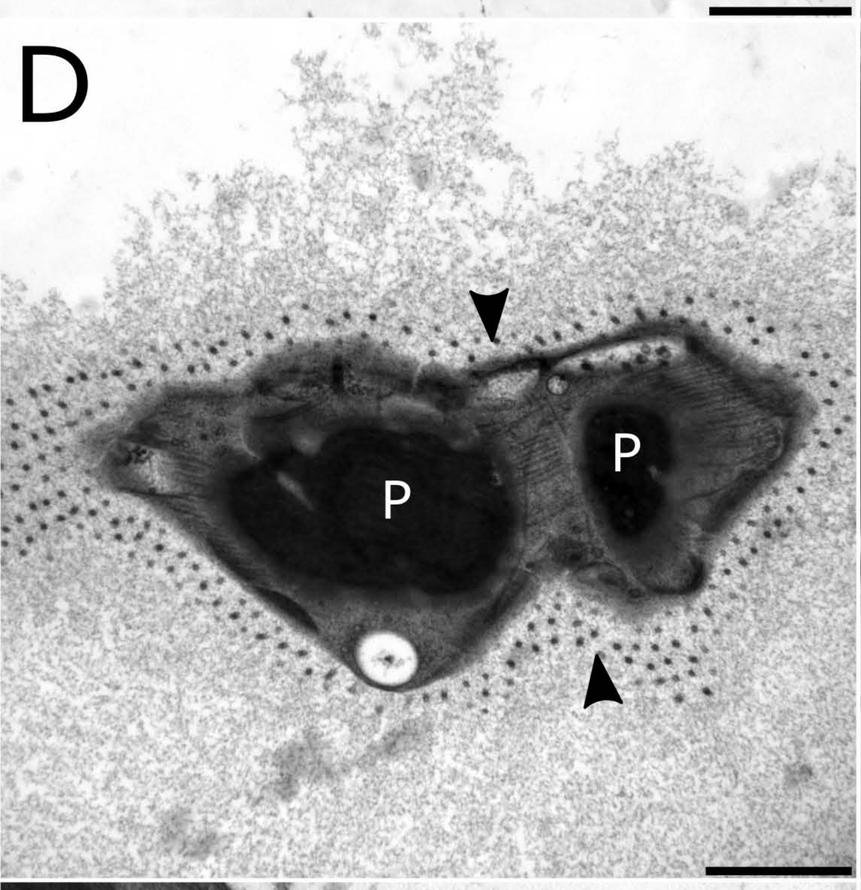
D
P
P
P

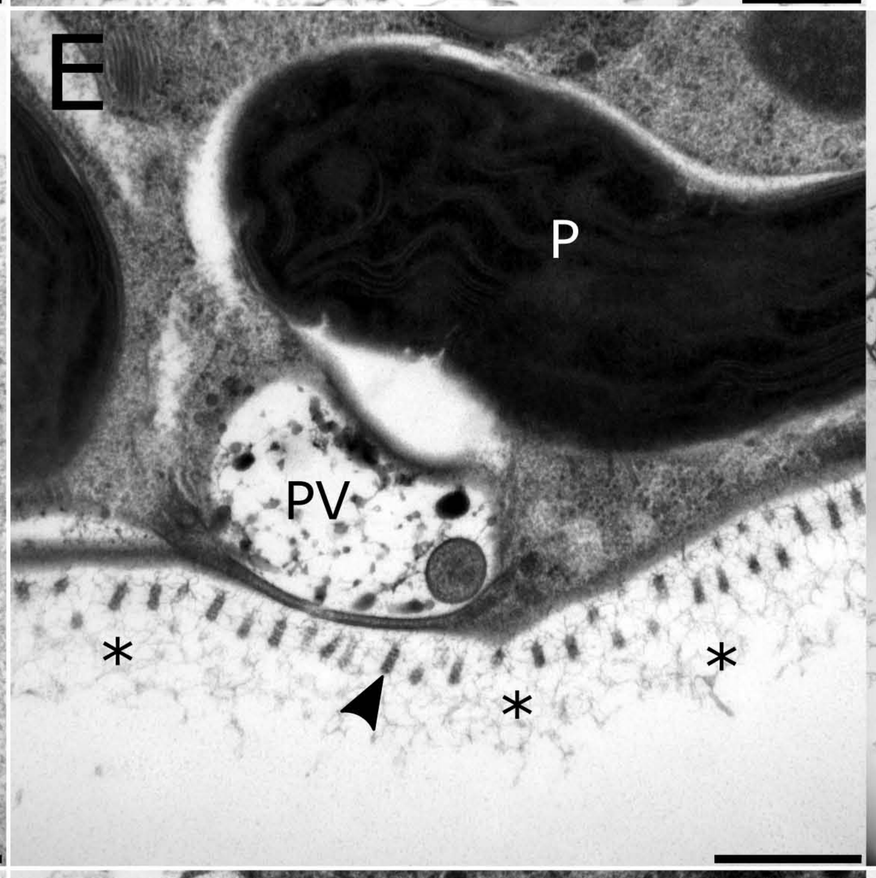
E
P
PV
*
*
*

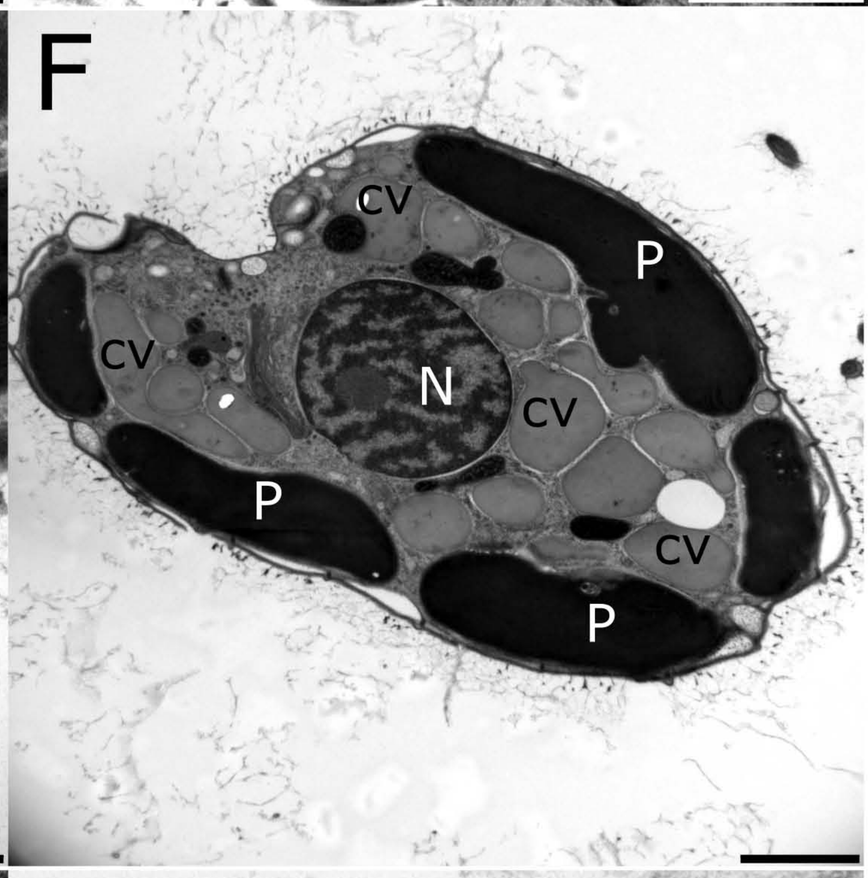
F
CV
P
CV
N
CV
P
CV
P

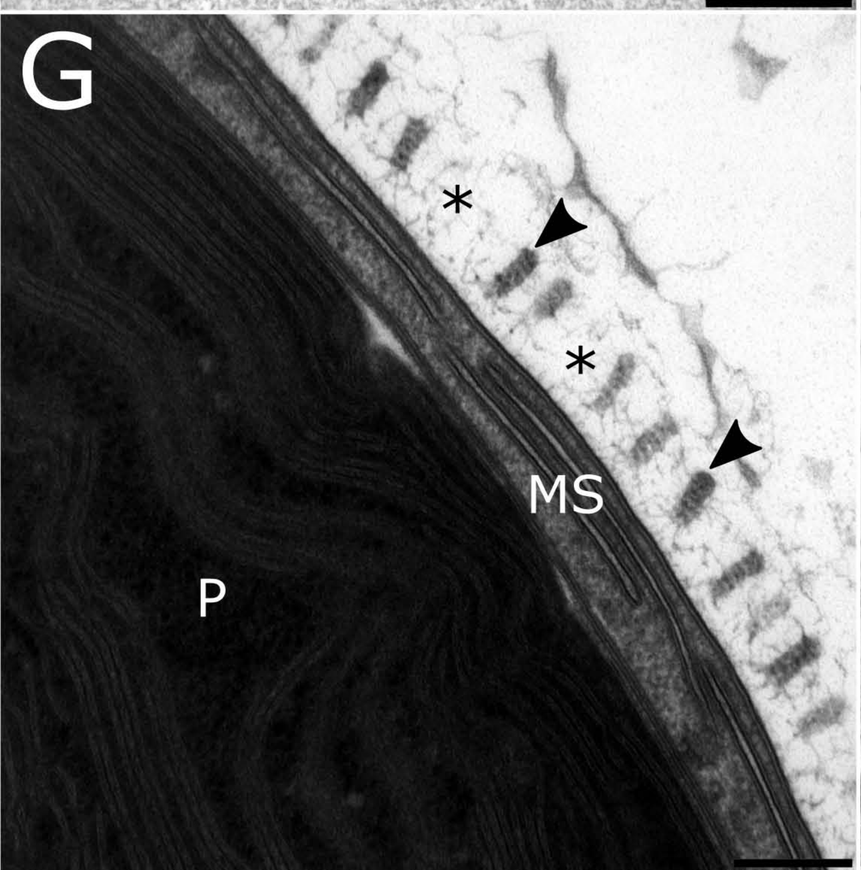
G
*
*
MS
P

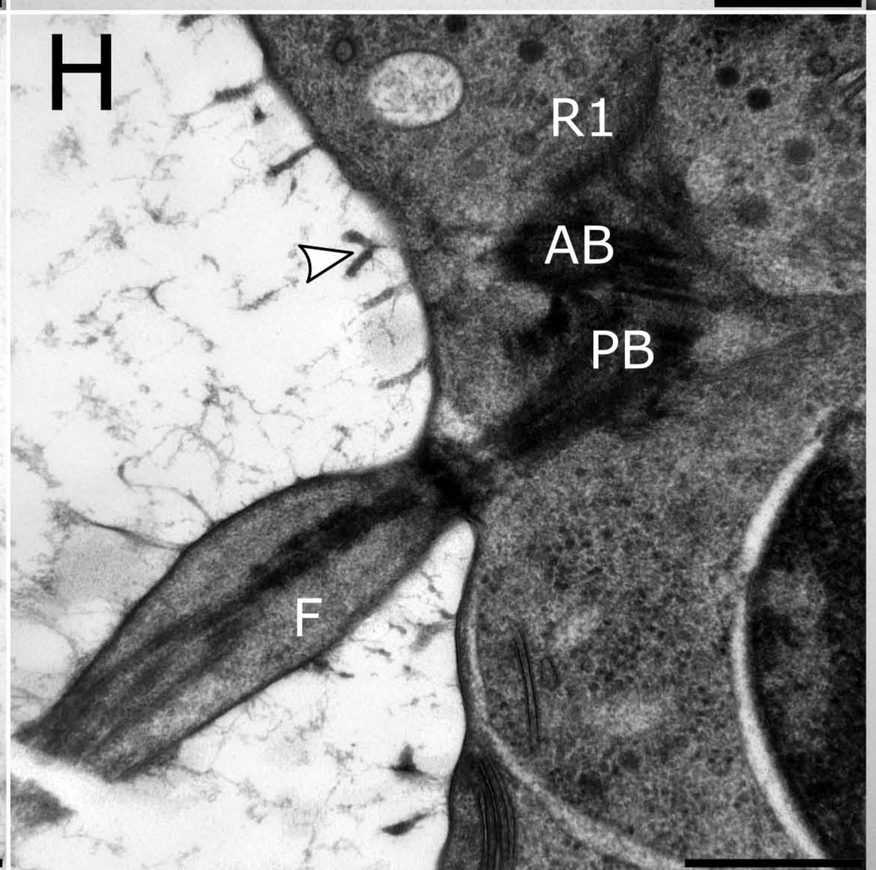
H
R1
AB
PB
F

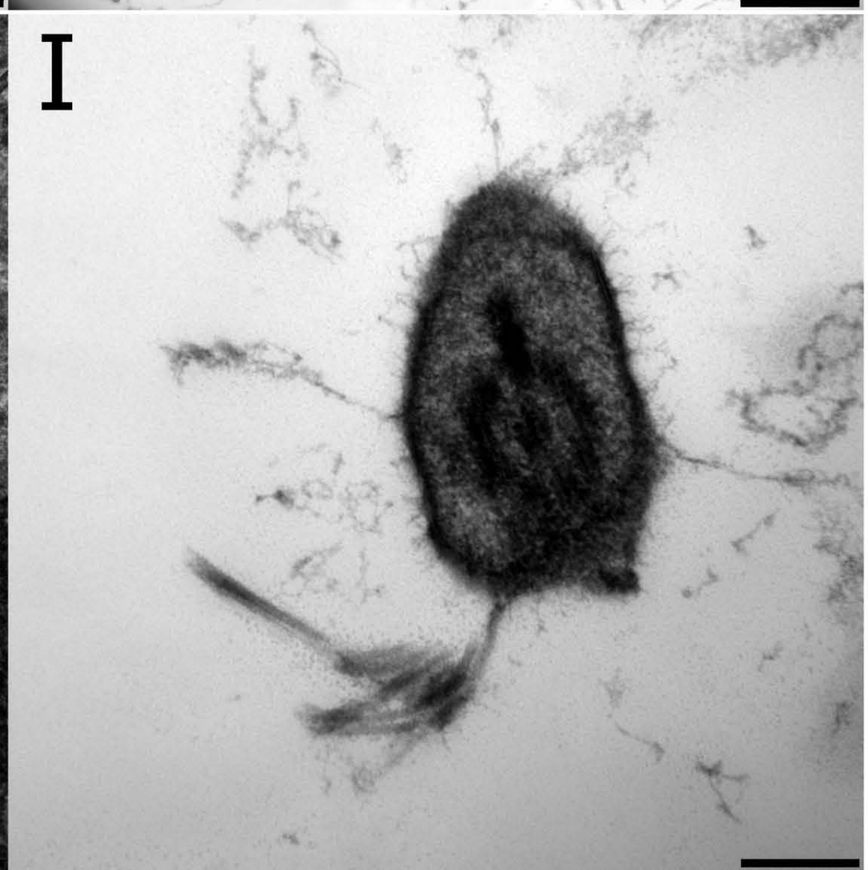
I

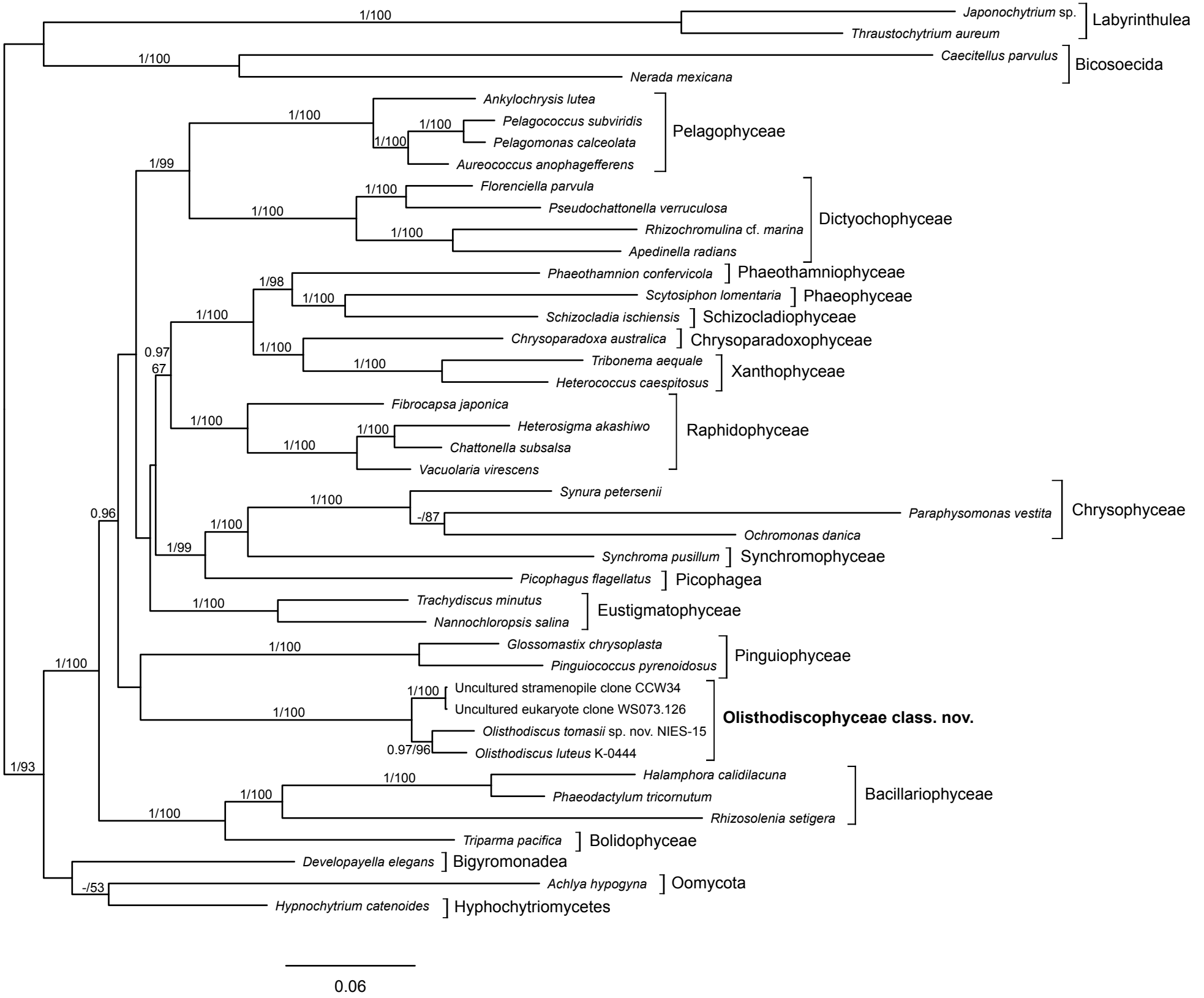
Japonochytrium sp.
Thraustochytrium aureum
Labyrinthulea
Caecitellus parvulus
Nerada mexicana
Bicosoecida
Ankylochrysis lutea
Pelagococcus subviridis
Pelagomonas calceolata
Aureococcus anophagefferens
Pelagophyceae
Florenciella parvula
Pseudochattonella verruculosa
Rhizochromulina cf. marina
Apedinella radians
Dictyochophyceae
Phaeothamnion confervicola
Phaeothamniophyceae
Scytosiphon lomentaria
Phaeophyceae
Schizocladia ischiensis
Schizocladiophyceae
Chrysoparadoxa australica
Chrysoparadoxophyceae
Tribonema aequale
Heterococcus caespitosus
Xanthophyceae
Fibrocapsa japonica
Heterosigma akashiwo
Chattonella subsalsa
Vacuolaria virescens
Raphidophyceae
Synura petersenii
Paraphysomonas vestita
Ochromonas danica
Chrysophyceae
Synchroma pusillum
Synchromophyceae
Picophagus flagellatus
Picophagea
Trachydiscus minutus
Nannochloropsis salina
Eustigmatophyceae
Glossomastix chrysoplasta
Pinguiococcus pyrenoidosus
Pinguiophyceae
Uncultured stramenopile clone CCW34
Uncultured eukaryote clone WS073.126
Olisthodiscus tomasii sp. nov. NIES-15
Olisthodiscus luteus K-0444
Olisthodiscophyceae class. nov.
Halamphora calidilacuna
Phaeodactylum tricornutum
Rhizosolenia setigera
Bacillariophyceae
Triparma pacifica
Bolidophyceae
Developayella elegans
Bigyromonadea
Achlya hypogyna
Oomycota
Hypnochytrium catenoides
Hyphochytriomycetes
1/100
1/100
1/100
1/100
1/100
1/99
1/100
1/100
1/98
1/100
1/100
0.97
67
1/100
1/100
1/100
1/100
1/100
0.96
1/100
-/87
1/99
1/100
1/100
1/100
1/100
1/100
1/100
0.97/96
1/93
1/100
1/100
1/100
-/53
0.06

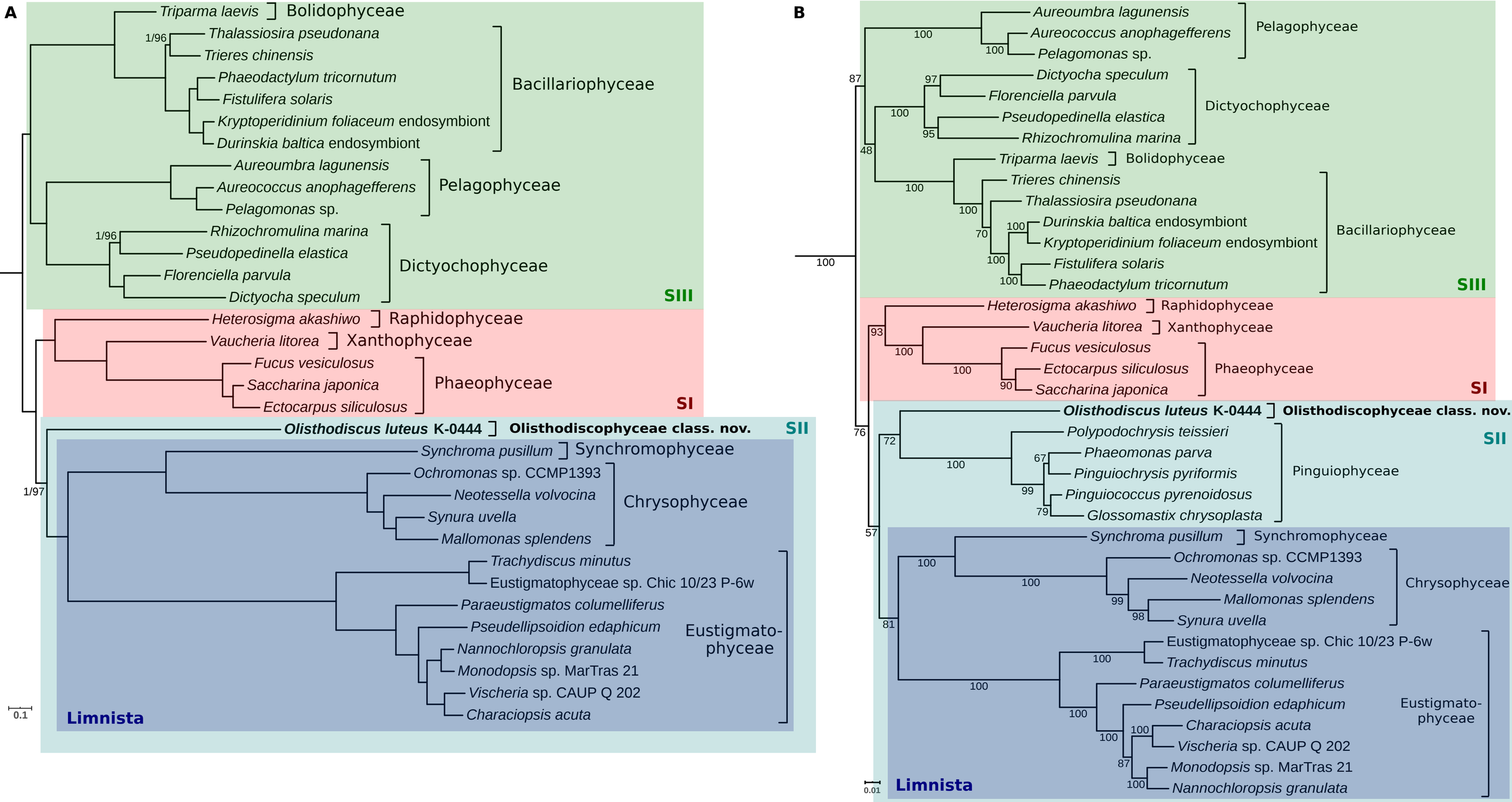
A
Triparma laevis
Bolidophyceae
1/96
Thalassiosira pseudonana
Trieres chinensis
Phaeodactylum tricornutum
Fistulifera solaris
Kryptoperidinium foliaceum endosymbiont
Durinskia baltica endosymbiont
Bacillariophyceae
Aureoumbra lagunensis
Aureococcus anophagefferens
Pelagomonas sp.
Pelagophyceae
1/96
Rhizochromulina marina
Pseudopedinella elastica
Florenciella parvula
Dictyocha speculum
Dictyochophyceae
SIII
Heterosigma akashiwo
Raphidophyceae
Vaucheria litorea
Xanthophyceae
Fucus vesiculosus
Saccharina japonica
Ectocarpus siliculosus
Phaeophyceae
SI
Olisthodiscus luteus K-0444
Olisthodiscophyceae class. nov.
SII
Synchroma pusillum
Synchromophyceae
1/97
Ochromonas sp. CCMP1393
Neotessella volvocina
Synura uvella
Mallomonas splendens
Chrysophyceae
Trachydiscus minutus
Eustigmatophyceae sp. Chic 10/23 P-6w
Paraeustigmatos columelliferus
Pseudellipsoidion edaphicum
Nannochloropsis granulata
Monodopsis sp. MarTras 21
Vischeria sp. CAUP Q 202
Characiopsis acuta
Eustigmato-phyceae
Limnista
0.1
B
Aureoumbra lagunensis
Aureococcus anophagefferens
Pelagomonas sp.
Pelagophyceae
Dictyocha speculum
Florenciella parvula
Pseudopedinella elastica
Rhizochromulina marina
Dictyochophyceae
Triparma laevis
Bolidophyceae
Trieres chinensis
Thalassiosira pseudonana
Durinskia baltica endosymbiont
Kryptoperidinium foliaceum endosymbiont
Fistulifera solaris
Phaeodactylum tricornutum
Bacillariophyceae
SIII
Heterosigma akashiwo
Raphidophyceae
Vaucheria litorea
Xanthophyceae
Fucus vesiculosus
Ectocarpus siliculosus
Saccharina japonica
Phaeophyceae
SI
Olisthodiscus luteus K-0444
Olisthodiscophyceae class. nov.
SII
Polypodochrysis teissieri
Phaeomonas parva
Pinguiochrysis pyriformis
Pinguiococcus pyrenoidosus
Glossomastix chrysoplasta
Pinguiophyceae
Synchroma pusillum
Synchromophyceae
Ochromonas sp. CCMP1393
Neotessella volvocina
Mallomonas splendens
Synura uvella
Chrysophyceae
Eustigmatophyceae sp. Chic 10/23 P-6w
Trachydiscus minutus
Paraeustigmatos columelliferus
Pseudellipsoidion edaphicum
Characiopsis acuta
Vischeria sp. CAUP Q 202
Monodopsis sp. MarTras 21
Nannochloropsis granulata
Eustigmato-phyceae
Limnista
0.01

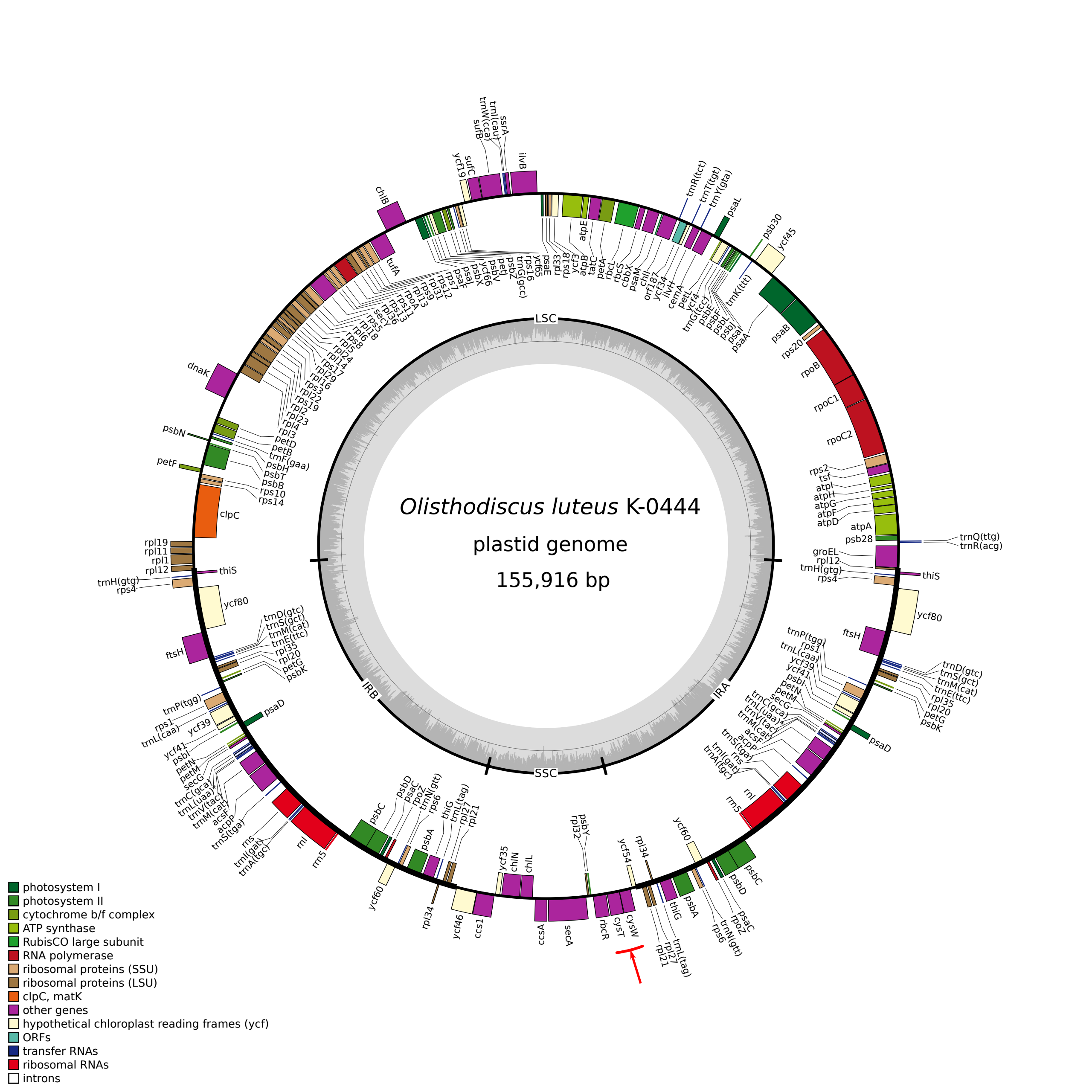
Olisthodiscus luteus K-0444
plastid genome
155,916 bp
LSC
IRB
IRA
SSC
photosystem I
photosystem II
cytochrome b/f complex
ATP synthase
RubisCO large subunit
RNA polymerase
ribosomal proteins (SSU)
ribosomal proteins (LSU)
clpC, matK
other genes
hypothetical chloroplast reading frames (ycf)
ORFs
transfer RNAs
ribosomal RNAs
introns

A

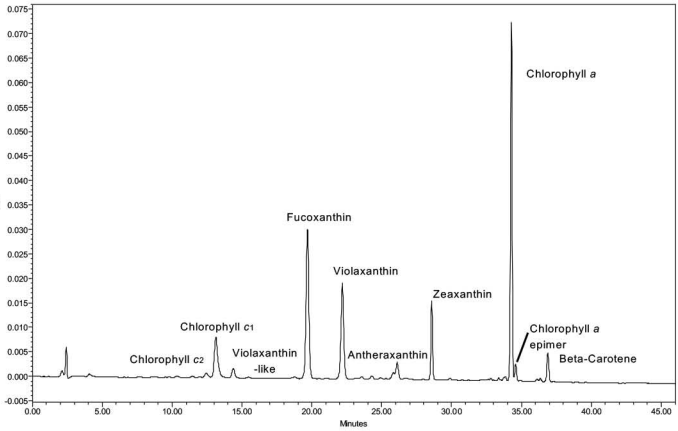
AU
Minutes
Chlorophyll a
Fucoxanthin
Violaxanthin
Zeaxanthin
Chlorophyll c1
Chlorophyll a epimer
Chlorophyll c2
Violaxanthin -like
Antheraxanthin
Beta-Carotene

B

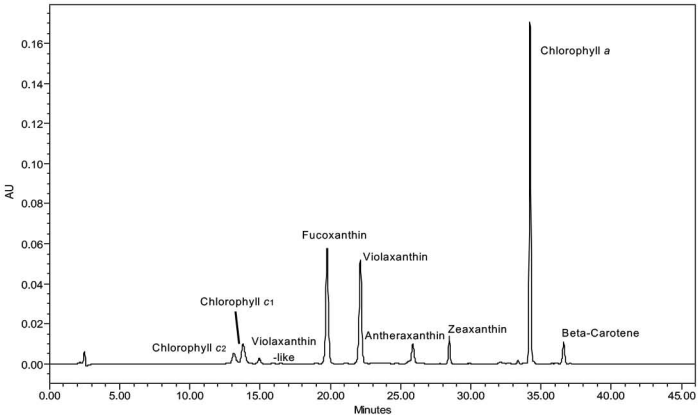
AU
Minutes
Chlorophyll a
Fucoxanthin
Violaxanthin
Chlorophyll c1
Chlorophyll c2
Violaxanthin -like
Antheraxanthin
Zeaxanthin
Beta-Carotene